 CMES, vol.78, no.2, pp.109-149, 2011

Generalized Westergaard Stress Functions as Fundamental Solutions

N.A. Dumont[1] **and E.Y. Mamani**[1]

Abstract: A particular implementation of the hybrid boundary element method is presented for the two-dimensional analysis of potential and elasticity problems, which, although general in concept, is suited for fracture mechanics applications. Generalized Westergaard stress functions, as proposed by Tada, Ernst and Paris in 1993, are used as the problem's fundamental solution. The proposed formulation leads to displacement-based concepts that resemble those presented by Crouch and Starfield, although in a variational framework that leads to matrix equations with clear mechanical meanings. Problems of general topology, such as in the case of unbounded and multiply-connected domains, may be modeled. The formulation, which is directly applicable to notches and generally curved, internal or external cracks, is specially suited for the description of the stress field in the vicinity of crack tips and is an easy means of evaluating stress intensity factors and of checking some basic concepts laid down by Rice in 1968. The paper focuses on the mathematical fundamentals of the formulation. One validating numerical example is presented.

Keywords: Westergaard stress functions, Hellinger-Reissner potential, hybrid boundary element, variational methods.

1 Introduction

Tada, Ernst, and Paris (1993, 1994) proposed a simple and efficient method of developing Westergaard stress functions for the analysis of displacement-prescribed and stress-prescribed crack problems. Their intervention was restricted to the mathematical means of arriving at the stress functions and the illustration of several forms of crack openings – always in terms of analytical developments.

The present paper makes use of Tada, Ernst and Paris' method and shows that such stress functions may be implemented as fundamental solutions of a generalized, two-dimensional boundary element method, and applied to problems that can be

[1] PUC-Rio, Brazil

completely unrelated to fracture mechanics. On the other hand, the formulation can be directly and advantageously applied to fracture mechanics [Dumont and Lopes (2003); Mamani (2011)].

Tada, Ernst and Paris' basic idea is extremely simple, as shown in Section 3. Although there is no claim of originality in the developments of the next Sections ([Dumont (2008)], see [Crouch and Starfield (1983)], for instance), they highlight some relevant mathematical aspects that Westergaard-like potential functions must satisfy to be applicable in the framework of an integral statement. Initially, a fundamental solution for potential problems is constructed and singularity issues are discussed [Dumont and Mamani (2011b)]. Then, the formulation is generalized to two-dimensional problems of elasticity [Dumont and Mamani (2011a)].

The traditional developments based on Westergaard stress functions work for a potential functional of the type $\Phi = \sigma_\infty z/\sqrt{z^2-a^2}$, which yields a constant stress $\sigma_\infty \neq 0$ at infinity. Results related to displacements are usually given in terms of the integral Φ^* of Φ. This potential function is also sometimes characterized as Z.

In the present outline, the method proposed by Tada, Ernst and Paris is used to define a non-dimensional potential function Φ that may have an in principle arbitrary configuration, depending on the local geometrical assumptions that are made, with all developments obtained in terms of Φ and its derivatives. Several configuration possibilities of Φ have been previously studied for the modeling of potential problems in a variational framework [Dumont (2008)]. In this paper, the potential function corresponds to the superposition of two elliptical half cracks, for a homogeneous slab of constant thickness under plane strain. The locally generated stresses and displacements (the latter ones evaluated except for rigid body displacements) tend to zero at a point that goes increasingly farther from the crack ($\sigma_\infty = 0$).

The primary motivation to the present theoretical developments was the evaluation of stress intensity factors in fracture mechanics. In spite of the superior analytical tools provided by the generalized Westergaard stress functions in the framework of a variational method [Lopes (2002); Dumont and Lopes (2003)], there seems to be no definitive answer to the question whether stress intensity factors can be automatically obtained within an arbitrarily high precision for an arbitrarily complicated elasticity problem. This issue was recently resumed by Mamani (2011) and is presently under investigation, although it is not the subject of the present paper.

This paper starts with a very brief outline of the hybrid boundary element method, as a representative formulation that can make use of the generalized Westergaard stress functions. In fact, there are several development possibilities of boundary element methods (variationally-based or not) in the present context, also in com-

bination with the Kelvin fundamental solution [Dumont and Lopes (2003)]. Then, the proposition by Tada, Ernst and Paris is briefly presented and developed for a general, rotated (semi-) crack configuration, which includes the assessment of all possible singularities. The formulation is initially applied to the solution of the Laplace equation. The core of the paper are the subsequent developments for plane elasticity, which are shown to be of exactly the same mathematical nature of the ones for potential problems. Numerical integration is outlined in an Appendix. A few academical, numerical examples are shown in order to validate the proposed developments and highlight some convergence issues.

2 Brief outline of the hybrid boundary element method

The hybrid boundary element method (HBEM) was introduced in 1987 on the basis of the Hellinger-Reissner potential and as a generalization of Pian's hybrid finite element method [Pian (1964); Dumont (1989)]. The formulation requires evaluation of integrals only along the boundary and makes use of fundamental solutions (Green's functions) to interpolate fields in the domain. Accordingly, an elastic body of arbitrary shape may be treated as a single finite macro-element with as many boundary degrees of freedom as desired. In the meantime, the formulation has evolved to several application possibilities, including time-dependent problems, fracture mechanics, non-homogeneous materials and strain gradient elasticity [Dumont and de Oliveira (2001); Dumont and Lopes (2003); Dumont, Chaves, and Paulino (2004); Dumont and Huamán (2009)].

2.1 Problem Formulation

Let an elastic body be submitted to tractions $\bar{t}_i$ on part Γ_σ of the boundary Γ and to displacements $\bar{u}_i$ on the complementary part Γ_u. For the sake of brevity, body forces are not included [Dumont (2011)]. One is attempting to find the best approximation for stresses and displacements, σ_{ij} and u_i, such that

$$\sigma_{ji,j} = 0 \quad \text{in the domain} \quad \Omega, \tag{1}$$

$$u_i = \bar{u}_i \quad \text{along} \quad \Gamma_u \quad \text{and} \quad t_i = \sigma_{ij} n_j = \bar{t}_i \quad \text{along} \quad \Gamma_\sigma \tag{2}$$

in which n_j is the outward unit normal to the boundary. Indicial notation is used.

2.2 Stress and Displacement Assumptions

Two independent trial fields are assumed [Pian (1964); Dumont (1989)]. The displacement field is explicitly approximated along the boundary by u_i^d, where $()^d$ means *displacement assumption*, in terms of polynomial functions u_{im} with compact support and nodal displacement parameters $\mathbf{d} = [d_m] \in \mathbb{R}^{n^d}$, for n^d displacement degrees of freedom of the discretized model. An independent stress field σ_{ij}^s,

where $()^s$ stands for *stress assumption*, is given in the domain in terms of a series of fundamental solutions σ^*_{ijm} with global support, multiplied by force parameters $\mathbf{p}^* = [p^*_m] \in \mathbb{R}^{n^*}$ applied at the same boundary nodal points m to which the nodal displacements d_m are attached ($n^* = n^d$).[1] Displacements u^s_i are obtained from σ^s_{ij}. Then,

$$u^d_i = u_{im}\, d_m \quad \text{on} \quad \Gamma \quad \text{such that} \quad u^d_i = \bar{u}_i \quad \text{on} \quad \Gamma_u \quad \text{and} \tag{3}$$

$$\sigma^s_{ij} = \sigma^*_{ijm}\, p^*_m \quad \text{such that} \quad \sigma^*_{jim,j} = 0 \quad \text{in} \quad \Omega \tag{4}$$

$$\Rightarrow \quad u^s_i = u^*_{im}\, p^*_m + u^r_{is}\, C_{sm}\, p^*_m \quad \text{in} \quad \Omega \tag{5}$$

where u^*_{im} are displacement fundamental solutions corresponding to σ^*_{ijm}. Rigid body motion is included in terms of functions u^r_{is} multiplied by in principle arbitrary constants C_{sm} [Dumont (2003, 2011)].

2.3 Governing Matrix Equations

The Hellinger-Reissner potential, based on the two-field assumptions of the latter section, as implemented by Pian (1964) and generalized by Dumont (1989), leads to two matrix equations that express nodal equilibrium and compatibility requirements. Dumont (2011) shows that the simplest, and still mathematically consistent, means of laying out these equations is in terms of two separately virtual works principles, as briefly presented in the following.

2.3.1 Displacement Virtual Work

In the absence of body forces, equilibrium is weakly enforced by

$$\int_\Omega \sigma^s_{ij}\, \delta u^d_{i,j}\, \mathrm{d}\Omega = \int_{\Gamma_\sigma} \bar{t}_i\, \delta u^d_i\, \mathrm{d}\Gamma \tag{6}$$

for $\sigma^s_{ij} = \sigma^s_{ji}$. Assuming that σ^s_{ij} is approximated according to Eq. (4) and that δu^d_i is given by Eq. (3), integration by parts of the term at the left-hand side of Eq. (6) and application of Green's theorem yield

$$\delta d_n \left[\int_\Gamma \sigma^*_{ijm}\, n_j\, u_{in}\, \mathrm{d}\Gamma - \int_\Omega \sigma^*_{ijm,j}\, u_{in}\, \mathrm{d}\Omega \right] p^*_m = \delta d_n \left[\int_\Gamma t_i\, u_{in}\, \mathrm{d}\Gamma \right] \tag{7}$$

[1] The denomination "fundamental solution" is used in a very broad sense, which comprises Green's and Trefftz functions. For Kelvin fundamental solutions, as in the conventional boundary element method and in the basic version of the HBEM, p^*_m are point forces. In the present outline, p^*_m are the resultants of forces applied at crack faces. The problem has the same mathematical format, although with different singularity issues. In a more generalized formulation, p^*_m may be just parameters with no special mechanical meaning [Dumont (2011); Dumont and Huamán (2009)].

Then, for arbitrary nodal displacements δd_n one obtains the matrix equilibrium equation

$$H_{mn}\, p^*_m = p_n \quad \text{or} \quad \mathbf{H}^{\mathrm{T}}\, \mathbf{p}^* = \mathbf{p} \tag{8}$$

in which $\mathbf{H} = [H_{nm}] \in \mathbb{R}^{n^d \times n^*}$, given by the first expression in brackets in Eq. (7), is the same double layer potential matrix of the collocation boundary element method [Brebbia, Telles, and Wrobel (1984)], and $\mathbf{p} = [p_n] \in \mathbb{R}^{n^d}$, given as the second term in brackets in Eq. (7), are equivalent nodal forces obtained as in the displacement finite element method. The domain integral of Eq. (7) is actually void, since σ^*_{ijm} are fundamental solutions, as in Eq. (4).

2.3.2 Stress virtual work

On the other hand, the displacement field u^d_i, explicitly approximated only along Γ according to Eq. (3), is made compatible with the domain displacement field u^s_i in terms of the following virtual work principle:

$$\int_\Omega \left(u^s_{i,j} - u^d_{i,j} \right) \delta\sigma^s_{ij}\, \mathrm{d}\Omega = 0 \tag{9}$$

for a virtual stress field $\delta\sigma^s_{ij}$ that is in equilibrium in Ω, according to Eq. (4).

Applying integration by parts and Green's theorem to the integral on the left-hand side of Equation (9), one arrives at

$$\int_\Gamma \left(u^s_i - u^d_i \right) \delta\sigma^*_{ij} \eta_j \mathrm{d}\Gamma - \int_\Omega \left(u^s_i - u^d_i \right) \delta\sigma^*_{ij,j}\, \mathrm{d}\Omega = 0 \tag{10}$$

This equation leads, after assuming that $\delta\sigma^s_{ij}$ is approximated according to Eq. (4) and that u^d_i is given by Eq. (3), to

$$F^*_{mn} p^*_n = H_{mn} d_n \quad \text{or} \quad \mathbf{F}^* \mathbf{p}^* \quad = \quad \mathbf{H}\mathbf{d} \tag{11}$$

where $\mathbf{H}$, which already appeared in Eq. (8), is recognized as performing a kinematic transformation, and $\mathbf{F}^* = [F^*_{nm}] \in \mathbb{R}^{n^* \times n^*}$ is a symmetric, flexibility matrix. The domain integration term in Eq. (11) is void, according to Eq. (4). The matrices $\mathbf{H}$ and $\mathbf{F}^*$ may be compactly defined as

$$[H_{mn} \quad F^*_{mn}] = \int_\Gamma \sigma^*_{ijm} n_j \, \langle u_{in} \quad u^*_{in} \rangle \, \mathrm{d}\Gamma \tag{12}$$

2.4 Problem solution with the hybrid boundary element method

Solving for $\mathbf{p}^*$ in Eqs. (8) and (11), one arrives at the matrix system

$$\mathbf{H}^{\mathrm{T}}\mathbf{F}^{*(-1)}\mathbf{H}\mathbf{d} = \mathbf{p} \tag{13}$$

where $\mathbf{H}^{\mathrm{T}}\mathbf{F}^{*(-1)}\mathbf{H} \equiv \mathbf{K}$ is a stiffness matrix. The inverse $\mathbf{F}^{*(-1)}$ must be carried out in terms of generalized inverses, as $\mathbf{F}^*$ is singular for a finite domain Ω [Dumont (2011)]. Results at internal points are expressed in terms of Eqs. (4) and (5) after evaluation of $\mathbf{p}^*$ in either Eq. (8) or (11).

For Neumann boundary conditions, only Eq. (8) is required, as occurs in the analysis of almost all fracture mechanics problems posed in the literature. This is the reason why in Sections 5.2 and 6.8 only the numerical integration of $\mathbf{H}$ is dealt with.

This Section presented a framework in which the generalized Westergaard functions of the subsequent Sections can be handled and applied. Alternative boundary element developments compatible with the use of Westergaard functions are possible [Dumont and Lopes (2003); Dumont (2011)].

3 Dislocation-based formulation by Tada, Ernst and Paris

Tada, Ernst, and Paris (1993) show that, for a prescribed crack opening of shape $f(x)$ in the interval $[x_1, x_2]$ along the x axis and symmetric with respect to this axis in the Cartesian coordinate system (x, y), one can define a potential function $\Phi(z)$ of the complex argument $z = x + iy$,

$$\Phi(z) = -\frac{1}{2\pi}\int_{x_1}^{x_2} \frac{f(x)}{z-x}\mathrm{d}x \tag{14}$$

and then obtain the corresponding stress and displacement functions, as a generalization of Westergaard's initial proposition in the frame of the fracture mechanics. Several crack and stress configurations are investigated by Tada, Ernst, and Paris (1993), as translation and superposition of effects can always be applied to compose intrincated crack patterns. Westergaard's developments for an elliptic crack opening of length $2a$ are obtained if one chooses the function

$$f(x) = \frac{\sqrt{a^2 - x^2}}{a} \tag{15}$$

and then carries out the integration of Eq. (14) in the interval $[-a, a]$.

4 Basics on a rotated semicrack

A very simple, although apparently original generalization of the above developments is obtained for a semicrack of length a_1 along a straight line that is rotated in the counter clock direction by an angle θ_1, Fig. 1, with which it is possible to compose kinked cracks of any length [Dumont (2008)], as developed in the rest of this paper. To make calculations as simple as possible, the crack shape function of Eq. (15), or any other shape, is initially defined for a semicrack length $a = 1$ and the integration of Eq. (14) is carried out in the interval $[0,1]$. Although the crack shape may be rather general, as given by Tada, Ernst, and Paris (1993) and as already explored in the present framework [Dumont (2008)], the ensuing developments are given for the elliptic semicrack corresponding to Eq. (15). The corresponding expression of Eq. (14) for the semicrack 1 is

$$\Phi_1 \equiv \Phi(Z_1) = -\frac{Z_1}{4} - \frac{1}{2\pi}\left(1 - \sqrt{1-Z_1^2}\ln\left(-\frac{1+\sqrt{1-Z_1^2}}{Z_1}\right)\right) \tag{16}$$

already given as argument of

$$Z_1 = zT_1 \equiv \frac{z}{a_1}e^{-i\theta_1} \equiv \frac{x+iy}{a_1}e^{-i\theta_1} \equiv \frac{r}{a_1}e^{i(\theta-\theta_1)} \tag{17}$$

from which the definition of the rotation and normalization term T_1 is inferred. The leading terms of Φ_1 at $Z_1 = 0$ (i. e., terms that are different from zero) are obtained

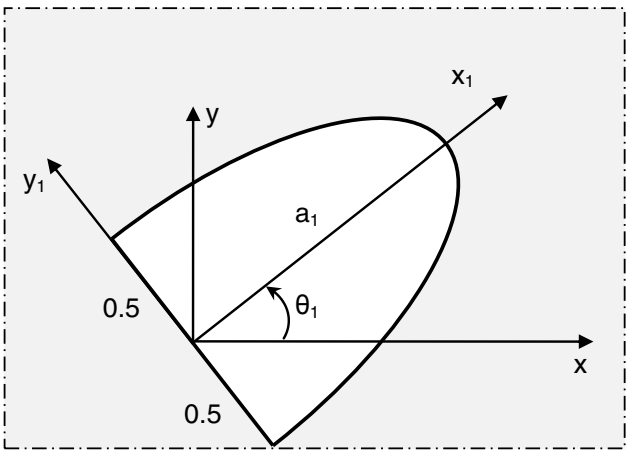

Figure 1: Semicrack of length a_1 rotated by an angle θ_1.

by series expansion,

$$\lim_{r\to 0}\Phi_1 = \frac{1}{2\pi}\left(-1+\ln(2)-\ln(Z_1)+i\,\pi\,\mathrm{csgn}\left(\frac{i\left(1+\sqrt{1-Z_1^2}\right)}{Z_1}\right)\right) \tag{18}$$

from which the real and imaginary parts are obtained, using $Z_1 = \dfrac{r}{a_1}\mathrm{e}^{i(\theta-\theta_1)}$:

$$\lim_{r\to 0}\mathrm{Re}\,\Phi_1 = \frac{-\ln(r)-1+\ln(2a_1)}{2\pi} \tag{19}$$

$$\lim_{r\to 0}\mathrm{Im}\,\Phi_1 = \begin{cases} \dfrac{\pi-\theta+\theta_1}{2\pi} & \text{for} \quad \theta_1 \le \theta \le \theta_1+\pi \\ \dfrac{-\pi-\theta+\theta_1}{2\pi} & \text{for} \quad \theta_1+\pi < \theta < \theta_1+2\pi \end{cases} \tag{20}$$

The first derivative of $\Phi(Z_1)$ with respect to Z_1 is

$$\Phi_1' \equiv \frac{\partial\Phi(Z_1)}{\partial Z_1} = -\frac{1}{2\pi}\left(Z_1\ln\left(-\frac{1+\sqrt{1-Z_1^2}}{Z_1}\right)\frac{1}{\sqrt{1-Z_1^2}}+\frac{1}{Z_1}+\frac{\pi}{2}\right) \tag{21}$$

The leading terms of Φ_1' at $Z_1 = 0$ are

$$\lim_{r\to 0}\Phi_1' = -\frac{1}{2\pi Z_1}-\frac{1}{4} \tag{22}$$

from which the real and imaginary parts are obtained:

$$\lim_{r\to 0}\mathrm{Re}\,\Phi_1' = -\frac{\cos(\theta-\theta_1)\,a_1}{2\pi r}-\frac{1}{4} \tag{23}$$

$$\lim_{r\to 0}\mathrm{Im}\,\Phi_1' = \frac{\sin(\theta-\theta_1)\,a_1}{2\pi r} \tag{24}$$

The second derivative of $\Phi(Z_1)$ with respect to Z_1 is

$$\Phi_1'' \equiv \frac{\partial^2\Phi(Z_1)}{\partial Z_1^2} = -\frac{1}{2\pi}\ln\left(-\frac{1+\sqrt{1-Z_1^2}}{Z_1}\right)\left(1-Z_1^2\right)^{-3/2}-\frac{1}{2\pi Z_1^2\left(-1+Z_1^2\right)} \tag{25}$$

The leading term of Φ_1'' at $Z_1 = 0$ is

$$\lim_{r\to 0}\Phi_1'' = \frac{1}{2\pi}\left(\frac{1}{Z_1^2} + \ln Z_1 + 1 - \ln 2 - i\,\pi\,\mathrm{csgn}\left(\frac{i\left(1+\sqrt{1-Z_1^2}\right)}{Z_1}\right)\right) \equiv \frac{1}{2\pi Z_1^2} - \lim_{r\to 0}\Phi_1 \tag{26}$$

and the corresponding real and imaginary parts are

$$\lim_{r\to 0}\mathrm{Re}\;\Phi_1'' = \frac{\cos(2\theta - 2\theta_1)\,a_1^2}{2\pi r^2} - \lim_{r\to 0}\mathrm{Re}\,\Phi_1 \tag{27}$$

$$\lim_{r\to 0}\mathrm{Im}\;\Phi_1'' = -\frac{\sin(2\theta - 2\theta_1)\,a_1^2}{2\pi r^2} - \lim_{r\to 0}\mathrm{Im}\,\Phi_1 \tag{28}$$

The functions Φ_1 and Φ_1' present at $Z_1 = 1$ singularities of the types $(Z_1^2-1)^{1/2}$ and $(Z_1^2-1)^{-1/2}$, as expected for the tip of an elliptic crack. This issue as well as the singularity of Φ_1'' at $Z_1 = 1$ are investigated later on in the opportune context.

5 Developments for a potential problem

The above developments are now applied to the derivation of a fundamental solution that can be used in the context of a hybrid boundary element method for potential problems. The developments in this Section are per se relevant and self contained. However, they serve as motivation to the more involved – and less intuitive – problem of elasticity.

5.1 Construction of a fundamental solution

A solution of the Laplace equation $\dfrac{\partial^2 u}{\partial x^2} + \dfrac{\partial^2 u}{\partial y^2} = 0$, say, for the steady-state heat transfer in a homogeneous plate of uniforme thickness t with coefficient of conductivity k, can be obtained from Φ_1, as introduced in Eq. (16), in terms of the potential

$$u_1 = \frac{1}{k}\mathrm{Im}\,\Phi_1 \tag{29}$$

with fluxes referred to the global Cartesian system (x,y)

$$\begin{aligned} q_{x_1} &= -k\frac{\partial u_1}{\partial x} = -\mathrm{Im}\,(T_1\Phi_1') \\ q_{y_1} &= -k\frac{\partial u_1}{\partial y} = -\mathrm{Re}\,(T_1\Phi_1') \end{aligned} \tag{30}$$

and normal flux

$$q_{n_1} = -q_{x_1} n_x - q_{y_1} n_y \quad \text{along} \quad \Gamma \tag{31}$$

where n_x and n_y are the projections of the boundary outward unit normal $\vec{n}$.

As formulated, u_1 is the temperature at a point (x, y) of the plate and q_{x_1} and q_{y_1} are heat fluxes – rate of heat transfer per unit surface area of the body – for a total heat flow input per plate thickness $Q/t = 1$, which comes out in the discussion after Eq. (40). The rotated Cartesian system of coordinates (x_1, y_1), as indicated in Fig. 1, is introduced with the purpose of arriving at a formal manipulation of the problem:

$$\begin{Bmatrix} x_1 \\ y_1 \end{Bmatrix} = \begin{bmatrix} \cos\theta_1 & \sin\theta_1 \\ -\sin\theta_1 & \cos\theta_1 \end{bmatrix} \begin{Bmatrix} x \\ y \end{Bmatrix}, \quad \text{or} \quad \mathbf{x}_1 = \mathbf{T}_1 \mathbf{x} \tag{32}$$

Then, the fluxes introduced in Eqs. (30) may also be expressed as

$$\begin{Bmatrix} q_{x_1} \\ q_{y_1} \end{Bmatrix} = \begin{bmatrix} \cos\theta_1 & -\sin\theta_1 \\ \sin\theta_1 & \cos\theta_1 \end{bmatrix} \begin{Bmatrix} q_{x_{1(0)}} \\ q_{y_{1(0)}} \end{Bmatrix}, \quad \text{or} \quad \mathbf{q}_1 = \mathbf{T}_1^{\mathrm{T}} \mathbf{q}_{1(0)} \tag{33}$$

where the subscript $()_{1(0)}$ indicates that the fluxes are referred to the Cartesian system (x_1, y_1) rotated by the angle θ_1:

$$\begin{aligned} q_{x_{1(0)}} &= -k \frac{\partial u_1}{\partial x_1} = -\frac{1}{a_1} \mathrm{Im}\,(\Phi_1') \\ q_{y_{1(0)}} &= -k \frac{\partial u_1}{\partial y_1} = -\frac{1}{a_1} \mathrm{Re}\,(\Phi_1') \end{aligned} \tag{34}$$

Let two segments of lengths a_1 and a_2 rotated by angles θ_1 and θ_2, respectively, compose lines of potential jumps (which correspond to lines of displacement discontinuities – cracks – in the elasticity case) along the boundary Γ of a body of domain Ω, with segment 1 coming before segment 2, in such a way that all phenomena along Γ are described in terms of a local variable ξ that runs in the counter clock direction, as illustrated in Fig. 2. The combined effect of the potential field is proposed as

$$u = u_1 - u_2 \tag{35}$$

with mathematical justification that follows immediately. According to Eq. (20), the latter equation leads to

$$\lim_{r\to 0} u \equiv \frac{1}{k} \lim_{r\to 0} \mathrm{Im}(\Phi_1 - \Phi_2) = \frac{1}{k} \begin{cases} \dfrac{\theta_1 - \theta_2}{2\pi} & \text{for } 0 \le \theta < \theta_1 \\ 1 + \dfrac{\theta_1 - \theta_2}{2\pi} & \text{for } \theta_1 \le \theta \le \theta_2 \\ \dfrac{\theta_1 - \theta_2}{2\pi} & \text{for } \theta_2 < \theta \le 2\pi \end{cases} \tag{36}$$

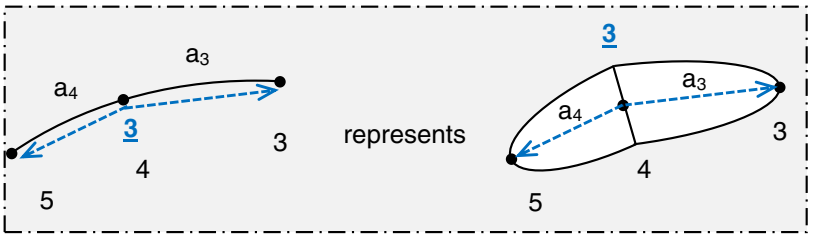

Figure 2: Representation of two semicracks that compose the crack element # 3 related to node # 4.

This is the same as expressing

$$\lim_{r\to 0} u \equiv \frac{1}{k}\lim_{r\to 0}\mathrm{Im}(\Phi_1-\Phi_2) = \frac{1}{k}\begin{cases} \dfrac{\theta_1-\theta_2}{2\pi} & \text{for a point outside } \Omega \\ 1+\dfrac{\theta_1-\theta_2}{2\pi} & \text{for a point inside } \Omega \end{cases} \tag{37}$$

The practical way to evaluate $\lim_{r\to 0} u = \dfrac{1}{k} + \dfrac{\theta_1-\theta_2}{2\pi k}$ for a point inside Ω, and for θ_1 and θ_2 in any quadrant, whenever required, is by writing $\lim_{r\to 0} u =$ frac $\left(1+\dfrac{\theta_1-\theta_2}{2\pi}\right)\dfrac{1}{k}$, observing that $0 < \lim_{r\to 0} u < \dfrac{1}{k}$.

5.1.1 Behavior of the normal flux along a crack or jump segment

One checks that, for the superposition of effects given in Eq. (35),

$$\lim_{r\to 0}\left(T_1\Phi_1' - T_2\Phi_2'\right) = -\frac{\mathrm{e}^{-i\theta_1}}{4a_1} + \frac{\mathrm{e}^{-i\theta_2}}{4a_2} \tag{38}$$

which is not only finite, but also independent from the angle θ along which the point $r=0$ is approached.

The projections of the outward unit normal $\vec{n}$, for Γ rotated by θ_1, are $n_x = \sin\theta_1$ and $n_y = -\cos\theta_1$. Then, for the combined effect of the potential field, as in Eq. (35), the normal flux q_n on Γ is

$$\lim_{r\to 0} q_n = \lim_{r\to 0}\left(-q_x n_x - q_y n_y\right) = \frac{1}{4a_1} - \frac{\cos(\theta_2-\theta_1)}{4a_2} \quad \text{along segment 1} \tag{39}$$

$$\lim_{r\to 0} q_n = \lim_{r\to 0}\left(-q_x n_x - q_y n_y\right) = \frac{1}{4a_2} - \frac{\cos(\theta_2-\theta_1)}{4a_1} \quad \text{along segment 2} \tag{40}$$

Observe that there is a jump in the value of q_n as one goes from one segment to the other. If $\theta_2 = \theta_1 + \pi$, that is, segments 1 and 2 constitute a straight boundary, both limits above result in $\lim_{r\to 0} q_n = \dfrac{1}{4a_1} + \dfrac{1}{4a_2}$, which means that there is no longer a jump, although q_n varies along the segments. Additionally, if $a_1 = a_2$, q_n is constant along the entire boundary segment and the integration of q_n along the segment results in a source of unit intensity, $Q/t = 1$.

Although there are no singularities at $r = 0$, the expressions of the potential u and of the flux q_n must be carefully assessed around the origin and at the opposite extremities of the segments 1 and 2, as numerical integrations are to be ultimately carried out for the evaluation of the matrices that result from a boundary element formulation. This is outlined in the Appendix.

5.1.2 *Behavior of the first derivative of the potential function along a crack or jump segment*

The derivative Φ' may be split for $Z = x$ in the interval $0 < x < 1$ into the following real and imaginary parts:

$$\Phi' = -\frac{1}{2\pi}\left(x \ln\left(\frac{1+\sqrt{1-x^2}}{x} \right) \frac{1}{\sqrt{1-x^2}} + \frac{1}{x} + \frac{\pi}{2} \right) \mp i \frac{x}{2\sqrt{1-x^2}}, \quad 0 < x < 1 \tag{41}$$

As shown in the former Section, the term $1/Z$, corresponding to $1/x$ above, cancels out when two segments are juxtaposed. The $(\mp)$ sign above depends on whether $y = 0^+$ or $y = 0^-$, with a jump at $y = 0$. From this equation and from the developments in the preceding sections one infers that $\mathrm{Re}\,\Phi'$ presents a logarithmic singularity at $x = 0$, as dealt with numerically in Section A.1, but tends smoothly to zero as the extremity $x = 1$ is reached, that is, $\mathrm{Re}\,\Phi'$ can be approach by a low-order polynomial close to the right extremity of the interval $0 < x < 1$. The imaginary part $\mathrm{Im}\,\Phi'$ has the opposite behavior, with a $1/\sqrt{1-x}$ singularity for $0 < x < 1$, but tending smoothly to zero as the extremity $x = 0$ is approached.

The following Section presents an algorithm for the numerical evaluation of Eq. (42) step by step along a segment $\overline{ij}$, for i varying from 1 to nn, the total number of boundary nodes, and j characterizing the node that succeeds i when one moves counterclockwise around the domain. When $k = i$ or $k = j$, the segment $\overline{ij}$ coincides with either $\overline{kk^+}$ or $\overline{k^-k}$ and there are in principle singularities on both extremities of the segment $\overline{ij}$, as a combination of the cases outlined in Sections A.1 and A.3. However, a simplification occurs for potential problems (as well as for elasticity, according to Section 6.7). For segment 1, for instance, the projections of the outward unit vector $\vec{n}$ are $n_x = \sin\theta_1$ and $n_y = -\cos\theta_1$. Then, one checks with use of

Eq. (33) that, in Eq. (42), $-q_{x_1}n_x - q_{y_1}n_y = q_{y_{1(0)}} = -\dfrac{1}{a_1}\mathrm{Re}\,(\Phi_1')$, which presents an implicit logarithmic singularity at $x_1 = 0$, but can be approximated by a low-order polynomial as $x_1 = a_1$ is approached. The fact that no singularity exists either at $x_1 = a_1$ along the segment 1 or at $x_2 = a_2$ along the segment 2 leads to the simple algorithm to be outlined next for the cases that $k = j$ or $k = i$.

5.2 *Numerical integration of the double-layer potential matrix H for potential problems*

The general expression of the double-layer potential matrix $\mathbf{H}$ is

$$\mathbf{H} \equiv H_{ki} = -\int_{\Gamma} (q_{x_k}n_x + q_{y_k}n_y)\, N_i |J|\, \mathrm{d}\xi \tag{42}$$

where k is the node of application of the potential source, i. e., the common node of two adjacent boundary segments, $\overline{k^- k}$ on the left (segment 1, rotated by an angle θ_1) and $\overline{kk^+}$ on the right (segment 2, rotated by an angle θ_2), as described in Section 5.1, and i is the node at which a potential of unit intensity is applied. The applied boundary potential varies linearly, according to the interpolation function N_i, from node i to the adjacent nodes on the left and on the right. Then, the integration interval indicated in the above equation comprehends, for the matrix coefficient H_{ki}, the two boundary segments that have i as common node (see Fig. 3). In this particular case, $|J|$ is the corresponding element length, for the natural boundary variable $\xi \in [0,1]$.

5.2.1 *Algorithm for the numerical integration of* $\mathbf{H}$

Let nn be the total number of nodes of a discretized model, which coincides with the total number of discretized boundary segments, as illustrated in Fig. 3. A body of any topology, with reentrant corners, holes and, after a slight modification of the basic code, also one-dimensional internal obstacles (which correspond to cracks in an elastic medium), can be simulated. The simulation of an internal crack is obtained as the modeling of a hole in the domain (then with node numbering running clockwise), as illustrated in the general numerical example of Fig. 6. However, as illustrated in Fig. 4 for a crack with n nodes, a fictitious node $n+3$ is introduced. After the numerical evaluation of all matrices, the rows and columns corresponding to nodes 1, $n+2$ and $n+3$ are removed and the effect of the internal crack is consistently taken into account [Mamani (2011); Dumont and Mamani (2011b,a)].

Define the matrices of potential functions and the matrix $\mathbf{N}$ of shape functions

$$\Phi' = \begin{bmatrix}\Phi_1' & \Phi_2'\end{bmatrix}, \quad \Phi'_{ln} = \begin{bmatrix}\Phi_1' & \Phi_2'\end{bmatrix}_{ln}, \quad \Phi'_{reg} = \begin{bmatrix}\Phi_1' & \Phi_2'\end{bmatrix}_{reg} \tag{43}$$

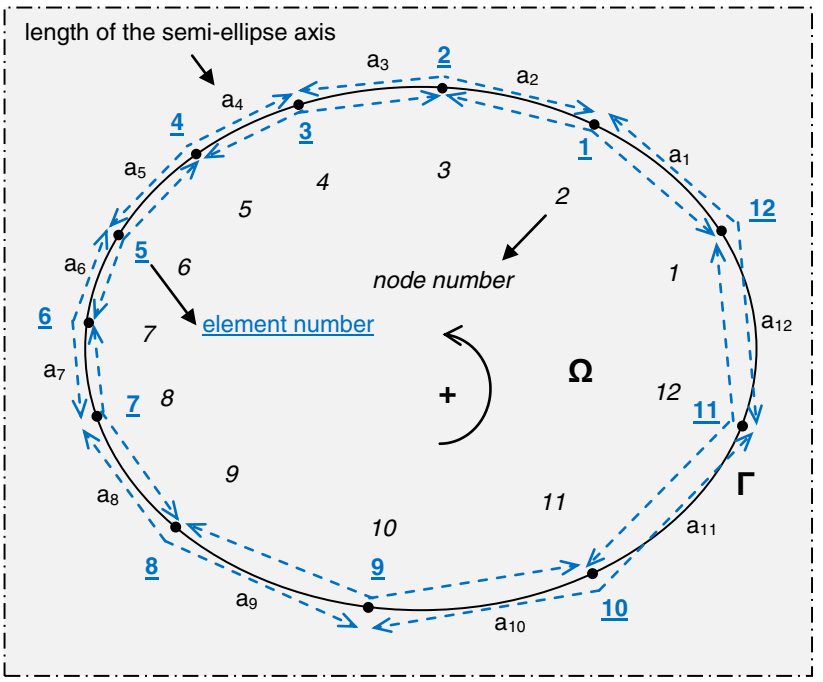

Figure 3: Illustration of a body discretized with 12 linear boundary elements and the corresponding definition of the crack segments.

$$\mathbf{N} = \begin{bmatrix} N_i & N_j \end{bmatrix} \equiv \begin{bmatrix} 1-\xi & \xi \end{bmatrix} \tag{44}$$

The subscripts $()_{ln}$ and $()_{reg}$ above indicate that the functions in the matrix coefficients are the ones defined in Eqs. (A.6) and (A.7), for the logarithmic singularity, and (A.18) and (A.19), for the $\sqrt{1/\xi}$ singularity. Moreover, define the $nn \times nn$ matrix $\mathbf{H}$ with all coefficients initially set as zero.

For the purpose of having the following algorithm as ready as possible for code writing, the coefficients of all matrices are referred to in brackets, whereas the primary variable is given in parentheses, such as $\Phi'(\xi)[c]$, where $c = 1,2$ for the first matrix in Eq. (43).

External loop for the *potential jumps* – corresponding to the *source cracks* in elasticity – with k varying from 1 to nn. Determine the adjacent nodes k^- and k^+, for the nodes numbered counterclockwise. Next, obtain $\cos\theta_1$, $\sin\theta_1$, $\cos\theta_2$, $\sin\theta_2$, according to Section 4.

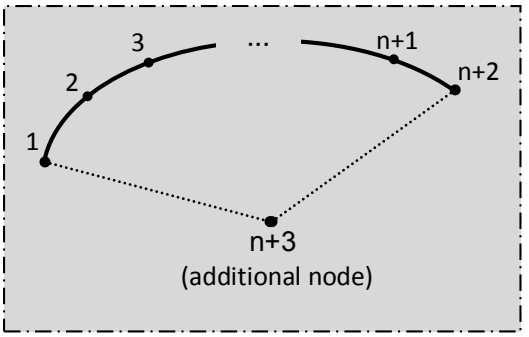

Figure 4: Fictitious node $n+3$ for the simulation of a curved crack with n segments.

Define the array of constants

$$\mathbf{C} = \begin{bmatrix} T_1 & -T_2 \end{bmatrix} \tag{45}$$

Internal loop for the *integration segments* **with** i **varying from 1 to** nn**.** Determine the subsequent node j, as integration will be carried out along the segment $\overline{ij}$.

Evaluate $x(\xi)$ and $y(\xi)$ along the segment $\overline{ij}$ as well as the derivatives $dx/d\xi$ and $dy/d\xi$ and the Jacobian $|J|$. Observe that, in Eq. (42), $n_x \mathrm{d}\Gamma = dy$ and $n_y \mathrm{d}\Gamma = -dx$. Next, evaluate $Z_1(\xi)$ and $Z_2(\xi)$, according to Eq. (17).

Carry out the numerical evaluation of the 2×2 complex array $\mathbf{h}$ in the following *logical if* structure using the procedures $lnproc()$ and $sqrtproc()$ given in the Appendix. In the loops to be presented, $c = 1,2$ refers to either semicrack 1 or 2, and $n = 1,2$ refers to either extremity i or j of a segment.

If $i = k$, then there is an embedded logarithmic singularity at the extremity $\xi = 0$ of the segment $\overline{ij}$ caused by the *potential jumps* along both segments $\overline{kk^+}$ and $\overline{k^-k}$: case (a) of Fig. 5.

For c and n varying from 1 to 2 in two nested loops,

Define $f = \Phi'(\xi)[c]\mathbf{N}(\xi)[n]$, $f_{ln} = \Phi'_{ln}(\xi)[c]\mathbf{N}(\xi)[n]$, $f_{reg} = f - f_{ln}\ln\xi$ and obtain $\mathbf{h}[n,c] = lnproc()$.

End of the nested loops with control variables c, n.

Else if $j = k$, then there is an embedded logarithmic singularity at the extremity $\xi = 1$ of the segment $\overline{ij}$ caused by the *potential jumps* along both segments $\overline{kk^+}$ and

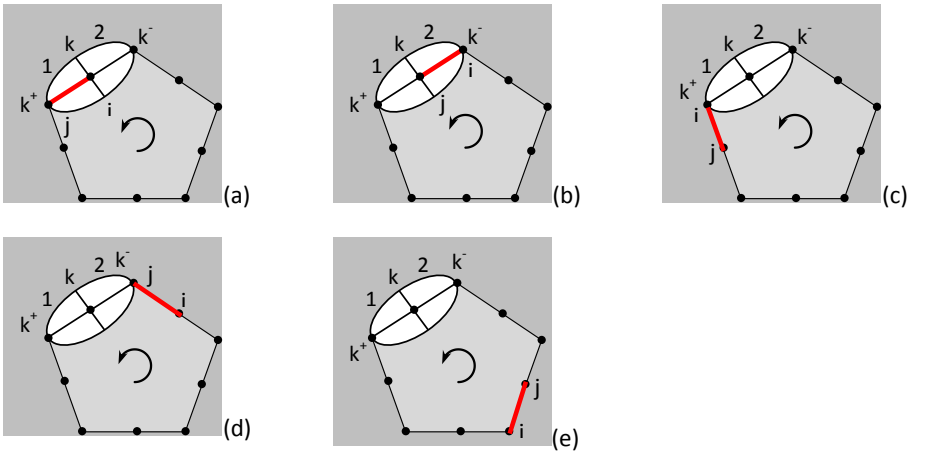

Figure 5: Illustration of the five cases to be taken into account in the numerical evaluation of the integral of Eqs. (42) and (93).

$\overline{k^- k}$: case (b) of Fig. 5.

For c and n varying from 1 to 2 in two nested loops,

Define $f = \Phi'(1-\xi)[c]\mathbf{N}(1-\xi)[n]$, $f_{ln} = \Phi'_{ln}(1-\xi)[c]\mathbf{N}(1-\xi)[n]$, $f_{reg} = f - f_{ln}\ln\xi$ and obtain $\mathbf{h}[n,c] = lnproc()$.

End of the nested loops with control variables c, n.

Else if $i = k^+$, then there is a square-root singularity at the extremity $\xi = 0$ of the segment $\overline{ij}$ caused by the *potential jump* 1 along the segment $\overline{kk^+}$: case (c) of Fig. 5. There is no singularity associated with the *potential jump* 2.

For n varying from 1 to 2,

Define $f = \Phi'(\xi)[1]\mathbf{N}(\xi)[n]$, $f_{reg} = \Phi'_{reg}(\xi)[1]\mathbf{N}(\xi)[n]$, $f_{sqrt} = (f - f_{reg})\sqrt{\xi}$ and obtain $\mathbf{h}[n,1] = sqrtproc()$.

Define $f = \Phi'(\xi)[2]\mathbf{N}(\xi)[n]$ and carry out the Gauss-Legendre quadrature $\mathbf{h}[n,2] = \sum_{i_g=1}^{n_g} f(\xi_g[i_g])w_g[i_g]$.

End of the loop with control variable n.

Else if $j = k^-$, then there is a square-root singularity at the extremity $\xi = 1$ of the segment $\overline{ij}$ caused by the *potential jump* 2 along the segment $\overline{k^- k}$: case (d) of Fig. 5. There is no singularity associated with the *potential jump* 1.

For n varying from 1 to 2,
Define $f = \Phi'(1-\xi)[2]\mathbf{N}(1-\xi)[n]$, $f_{reg} = \Phi'_{sqrt}(1-\xi)[2]\mathbf{N}(1-\xi)[n]$, $f_{sqrt} = (f - f_{reg})\sqrt{\xi}$ and obtain $\mathbf{h}[n,2] = sqrt\,proc()$.
Define $f = \Phi'(\xi)[1]\mathbf{N}(\xi)[n]$ and carry out the Gauss-Legendre quadrature $\mathbf{h}[n,1] = \sum_{i_g=1}^{n_g} f(\xi_g[i_g])w_g[i_g]$.
End of the nested loops with control variable n.

Else there is no singularity: case (e) of Fig. 5.
For c and n varying from 1 to 2 in two nested loops,
Define $f = \Phi'(\xi)[c]\mathbf{N}(\xi)[n]$ and carry out the Gauss-Legendre quadrature $\mathbf{h}[n,c] = \sum_{i_g=1}^{n_g} f(\xi_g[i_g])w_g[i_g]$.
End of the nested loops with control variables c, n.

End if End of the *structured logical if.*
Define the matrix of boundary unit projections referred to the segment $\overline{ij}$, as introduced in Eq. (31),

$$\mathbf{n} = \begin{bmatrix} n_x & n_y \end{bmatrix} \tag{46}$$

The coefficient H_{coef} of the matrix $\mathbf{H}$ in Eq. (42) is obtained in the following loop, according to Eq. (31), for nodes i and j given in the array $\mathbf{i} \equiv [i, j]$.

Loop for extremities i and j, with n varying from 1 to 2

$$H_{coef} = \left[\sum_{c=1}^{2} \mathbf{C}[c,1]\,\mathrm{Im}(\mathbf{h}[n,c]) + \mathbf{C}[c,2]\,\mathrm{Re}(\mathbf{h}[n,c]) \right] \mathbf{n}^{\mathrm{T}} \tag{47}$$

The matrix $\mathbf{H}$, whose coefficients may already have contribution from a preceding integration over an adjacent segment, is obtained from $\mathbf{H}_{sub}[n]$ as

$$\mathbf{H}[k, \mathbf{i}[n]] = \mathbf{H}[k, \mathbf{i}[n]] + H_{coef} \tag{48}$$

End of loops with control variables n, i, k.

6 Developments for elasticity problems

6.1 Developments for a mode I stress state

The expressions of displacements $\mathbf{u}_1^I$ and stresses σ_1^I for a crack rotated by an angle θ_1, as referred to the global coordinates (x,y), are, for mode I,

$$
\begin{aligned}
&u_1^I = \\
&\frac{1+\nu}{E}\left[(1-2\nu)\cos\theta_1 \operatorname{Re}\Phi_1 - 2(1-\nu)\sin\theta_1 \operatorname{Im}\Phi_1 + \frac{y_1}{a_1}\left(\sin\theta_1 \operatorname{Re}\Phi_1' - \cos\theta_1 \operatorname{Im}\Phi_1'\right)\right] \\
&v_1^I = \\
&\frac{1+\nu}{E}\left[(1-2\nu)\sin\theta_1 \operatorname{Re}\Phi_1 + 2(1-\nu)\cos\theta_1 \operatorname{Im}\Phi_1 - \frac{y_1}{a_1}\left(\cos\theta_1 \operatorname{Re}\Phi_1' - \sin\theta_1 \operatorname{Im}\Phi_1'\right)\right] \\
&\sigma_{xx_1}^I = \frac{1}{a_1}\operatorname{Re}\Phi_1' + \frac{y_1}{a_1^2}\left(\sin 2\theta_1 \operatorname{Re}\Phi_1'' - \cos 2\theta_1 \operatorname{Im}\Phi_1''\right) \\
&\sigma_{yy_1}^I = \frac{1}{a_1}\operatorname{Re}\Phi_1' - \frac{y_1}{a_1^2}\left(\sin 2\theta_1 \operatorname{Re}\Phi_1'' - \cos 2\theta_1 \operatorname{Im}\Phi_1''\right) \\
&\tau_{xy_1}^I = -\frac{y_1}{a_1^2}\left(\cos 2\theta_1 \operatorname{Re}\Phi_1'' + \sin 2\theta_1 \operatorname{Im}\Phi_1''\right)
\end{aligned}
\tag{49}
$$

where

$$
y_1 = y\cos\theta_1 - x\sin\theta_1 \equiv r\sin(\theta-\theta_1) \tag{50}
$$

The displacement and stress expressions can be given in a more compact and understandable format. For a crack rotated by an angle θ_1, with rotated coordinates

$$
\begin{Bmatrix} x_1 \\ y_1 \end{Bmatrix} = \begin{bmatrix} \cos\theta_1 & \sin\theta_1 \\ -\sin\theta_1 & \cos\theta_1 \end{bmatrix} \begin{Bmatrix} x \\ y \end{Bmatrix}, \quad \text{or} \quad \mathbf{x}_1 = \mathbf{T}_1\mathbf{x} \tag{51}
$$

the displacement vector $\mathbf{u}_{1(0)}^I$ and the stress tensor $\sigma_{1(0)}^I$ are

$$
\mathbf{u}_{1(0)}^I = \frac{1+\nu}{E}\begin{Bmatrix} (1-2\nu)\operatorname{Re}\Phi_1 - \dfrac{y_1}{a_1}\operatorname{Im}\Phi_1' \\ 2(1-\nu)\operatorname{Im}\Phi_1 - \dfrac{y_1}{a_1}\operatorname{Re}\Phi_1' \end{Bmatrix} \tag{52}
$$

$$
\sigma_{1(0)}^I = \begin{bmatrix} \dfrac{1}{a_1}\operatorname{Re}\Phi_1' - \dfrac{y_1}{a_1^2}\operatorname{Im}\Phi_1'' & -\dfrac{y_1}{a_1^2}\operatorname{Re}\Phi_1'' \\ -\dfrac{y_1}{a_1^2}\operatorname{Re}\Phi_1'' & \dfrac{1}{a_1}\operatorname{Re}\Phi_1' + \dfrac{y_1}{a_1^2}\operatorname{Im}\Phi_1'' \end{bmatrix} \tag{53}
$$

where the subscript $(\,)_{1(0)}$ refers to direction θ_1, but with displacements and stresses locally oriented. Then, the results of Eq. (49) are

$$\mathbf{u}_1^I = \mathbf{T}_1^{\mathrm{T}} \mathbf{u}_{1(0)}^I \tag{54}$$

$$\sigma_1^I = \mathbf{T}_1^{\mathrm{T}} \sigma_{1(0)}^I \mathbf{T}_1 \tag{55}$$

It is convenient to express the above equation for the stress coefficients aligned as a vector:

$$\begin{Bmatrix} \sigma^I_{xx_1} \\ \sigma^I_{yy_1} \\ \tau^I_{xy_1} \end{Bmatrix} = \begin{bmatrix} \cos^2\theta_1 & \sin^2\theta_1 & -\sin 2\theta_1 \\ \sin^2\theta_1 & \cos^2\theta_1 & \sin 2\theta_1 \\ \sin 2\theta_1/2 & -\sin 2\theta_1/2 & \cos 2\theta_1 \end{bmatrix} \begin{Bmatrix} \sigma^I_{xx_{1(0)}} \\ \sigma^I_{yy_{1(0)}} \\ \tau^I_{xy_{1(0)}} \end{Bmatrix} \tag{56}$$

6.2 Developments for a mode II stress state

The expressions for displacements $\mathbf{u}_1^{II}$ and stresses σ_1^{II} for a crack rotated by an angle θ_1, as referred to the global coordinates (x,y), are, for mode II,

$$\begin{aligned}
&u_1^{II} = \\
&\frac{1+\nu}{E}\left[(1-2\nu)\sin\theta_1 \operatorname{Re}\Phi_1 + 2(1-\nu)\cos\theta_1 \operatorname{Im}\Phi_1 + \frac{y_1}{a_1}\left(\cos\theta_1 \operatorname{Re}\Phi_1' + \sin\theta_1 \operatorname{Im}\Phi_1'\right)\right] \\
&v_1^{II} = \\
&\frac{1+\nu}{E}\left[-(1-2\nu)\cos\theta_1 \operatorname{Re}\Phi_1 + 2(1-\nu)\sin\theta_1 \operatorname{Im}\Phi_1 + \frac{y_1}{a_1}\left(\sin\theta_1 \operatorname{Re}\Phi_1' - \cos\theta_1 \operatorname{Im}\Phi_1'\right)\right] \\
&\sigma^{II}_{xx_1} = \frac{1}{a_1}\left[-\sin 2\theta_1 \operatorname{Re}\Phi_1' + (1+\cos 2\theta_1)\operatorname{Im}\Phi_1'\right] + \frac{y_1}{a_1^2}\left(\cos 2\theta_1 \operatorname{Re}\Phi_1'' + \sin 2\theta_1 \operatorname{Im}\Phi_1''\right) \\
&\sigma^{II}_{yy_1} = \frac{1}{a_1}\left[\sin 2\theta_1 \operatorname{Re}\Phi_1' + (1-\cos 2\theta_1)\operatorname{Im}\Phi_1'\right] - \frac{y_1}{a_1^2}\left(\cos 2\theta_1 \operatorname{Re}\Phi_1'' + \sin 2\theta_1 \operatorname{Im}\Phi_1''\right) \\
&\tau^{II}_{xy_1} = \frac{1}{a_1}\left[\cos 2\theta_1 \operatorname{Re}\Phi_1' + \sin 2\theta_1 \operatorname{Im}\Phi_1'\right] + \frac{y_1}{a_1^2}\left(\sin 2\theta_1 \operatorname{Re}\Phi_1'' - \cos 2\theta_1 \operatorname{Im}\Phi_1''\right)
\end{aligned} \tag{57}$$

As developed for mode I, these expressions can be given in a more compact and understandable format. For a crack rotated by an angle θ_1, according to Eq. (51) the displacements $\mathbf{u}_{1(0)}^{II}$ and stresses $\sigma_{1(0)}^{II}$ are

$$\mathbf{u}^{II}_{1(0)} = \frac{1+\nu}{E}\begin{Bmatrix} 2(1-\nu)\operatorname{Im}\Phi_1 + \dfrac{y_1}{a_1}\operatorname{Re}\Phi_1' \\ -(1-2\nu)\operatorname{Re}\Phi_1 - \dfrac{y_1}{a_1}\operatorname{Im}\Phi_1' \end{Bmatrix} \tag{58}$$

$$\sigma^{II}_{1(0)} = \begin{bmatrix} \dfrac{2}{a_1}\,\mathrm{Im}\,\Phi_1' + \dfrac{y_1}{a_1^2}\,\mathrm{Re}\,\Phi_1'' & \dfrac{1}{a_1}\,\mathrm{Re}\,\Phi_1' - \dfrac{y_1}{a_1^2}\,\mathrm{Im}\,\Phi_1'' \\ \dfrac{1}{a_1}\,\mathrm{Re}\,\Phi_1' - \dfrac{y_1}{a_1^2}\,\mathrm{Im}\,\Phi_1'' & -\dfrac{y_1}{a_1^2}\,\mathrm{Re}\,\Phi_1'' \end{bmatrix} \tag{59}$$

where the subscript $(\,)_{1(0)}$ refers to direction θ_1, but with displacements and stresses locally oriented. Then, the results of Eq. (57) are

$$\mathbf{u}_1^{II} = \mathbf{T}_1^{\mathrm{T}}\mathbf{u}_{1(0)}^{II} \tag{60}$$

$$\sigma_1^{II} = \mathbf{T}_1^{\mathrm{T}}\sigma_{1(0)}^{II}\mathbf{T}_1 \tag{61}$$

The above result may also be expressed as in Eq. (56).

6.3 Compact expressions of displacements and stresses for modes I and II

The displacements and stresses due to the combined actions of mode I and mode II at crack 1, for applied crack forces of intensity p_1^I and p_1^{II}, are compactly expressed as

$$\begin{Bmatrix} u_1 \\ v_1 \end{Bmatrix} = \begin{bmatrix} \cos\theta_1 & -\sin\theta_1 \\ \sin\theta_1 & \cos\theta_1 \end{bmatrix} \begin{bmatrix} u^I_{1(0)} & u^{II}_{1(0)} \\ v^I_{1(0)} & v^{II}_{1(0)} \end{bmatrix} \begin{Bmatrix} p_1^I \\ p_1^{II} \end{Bmatrix}, \quad \text{or} \quad \mathbf{u}_1 = \mathbf{T}_1^{\mathrm{T}}\mathbf{u}_{1(0)}\mathbf{p}_1 \tag{62}$$

$$\begin{Bmatrix} \sigma_{xx_1} \\ \sigma_{yy_1} \\ \tau_{xy_1} \end{Bmatrix} = \begin{bmatrix} \cos^2\theta_1 & \sin^2\theta_1 & -\sin 2\theta_1 \\ \sin^2\theta_1 & \cos^2\theta_1 & \sin 2\theta_1 \\ \sin 2\theta_1/2 & -\sin 2\theta_1/2 & \cos 2\theta_1 \end{bmatrix} \begin{bmatrix} \sigma^I_{xx_{1(0)}} & \sigma^{II}_{xx_{1(0)}} \\ \sigma^I_{yy_{1(0)}} & \sigma^{II}_{yy_{1(0)}} \\ \tau^I_{xy_{1(0)}} & \tau^{II}_{xy_{1(0)}} \end{bmatrix} \begin{Bmatrix} p_1^I \\ p_1^{II} \end{Bmatrix}, \tag{63}$$

or $\sigma_1 = \mathbf{R}_1\sigma_{1(0)}\mathbf{p}_1$

All results above have been checked using Maple™, for a general complex function Φ, making sure that displacements and stresses correspond to each other, for plane strain state, and that the stresses are in equilibrium. The manipulation of complex functions is best done in terms of $\mathrm{Re}\,\Phi = \dfrac{\Phi+\bar{\Phi}}{2}$ and $\mathrm{Im}\,\Phi = -i\dfrac{\Phi-\bar{\Phi}}{2}$. The stress results were obtained as general real functions $f(x,y) = \dfrac{1}{2}\left[(a+ib)\,\Phi + (a-ib)\,\bar{\Phi}\right]$ and then converted to $f(x,y) = a\,\mathrm{Re}\,\Phi - b\,\mathrm{Im}\,\bar{\Phi}$.

6.4 Condition for the actions of the combined semicracks 1 and 2 to be finite

The developments above have been done for a crack rotated by an angle θ_1. For the combined action of two cracks rotated with angles θ_1 and θ_2, the displacements are

given as the superposition of effects:

$$\begin{Bmatrix} u \\ v \end{Bmatrix} = \begin{bmatrix} u_1^I & u_1^{II} \\ v_1^I & v_1^{II} \end{bmatrix} \begin{Bmatrix} p_1^I \\ p_1^{II} \end{Bmatrix} + \begin{bmatrix} u_2^I & u_2^{II} \\ v_2^I & v_2^{II} \end{bmatrix} \begin{Bmatrix} p_2^I \\ p_2^{II} \end{Bmatrix} \quad \text{or} \quad \mathbf{u} = \mathbf{T}_1^{\mathrm{T}} \mathbf{u}_{1(0)} \mathbf{p}_1 + \mathbf{T}_2^{\mathrm{T}} \mathbf{u}_{2(0)} \mathbf{p}_2 \tag{64}$$

The leading terms of displacements $\mathbf{u}_{1(0)}$ for the semicrack 1 are:

$$\lim_{r\to 0} u_{1(0)}^I = \frac{1+\nu}{2\pi E} \left((1-2\nu)\left(-\ln(r) - 1 + \ln(2a_1)\right) - \sin(\Delta_1)^2 \right) \tag{65}$$

$$\lim_{r\to 0} v_{1(0)}^I = \frac{1+\nu}{2\pi E} \left(-2(1-\nu)\left(\Delta_1 + \operatorname{csgn}\left(i\sin(\Delta_1) - \cos(\Delta_1)\right)\pi\right) + \sin(\Delta_1)\cos(\Delta_1)\right) \tag{66}$$

$$\lim_{r\to 0} u_{1(0)}^{II} = \frac{1+\nu}{2\pi E} \left(-2(1-\nu)\left(\Delta_1 + \operatorname{csgn}\left(i\sin(\Delta_1) - \cos(\Delta_1)\right)\pi\right) - \sin(\Delta_1)\cos(\Delta_1)\right) \tag{67}$$

$$\lim_{r\to 0} v_{1(0)}^{II} = \frac{1+\nu}{2\pi E} \left((1-2\nu)\left(\ln(r) + 1 - \ln(2a_1)\right) - \sin(\Delta_1)^2 \right) \tag{68}$$

where $\Delta_1 = \theta - \theta_1$. The leading terms of displacements $\mathbf{u}_{2(0)}$ for the semicrack 2 have the same expressions above if a_2 and Δ_2 are substituted for a_1 and Δ_1.

The condition for the combined action of the semicracks 1 and 2 to be finite is obtained by enforcing that the term that multiplies $\ln r$ in u and v in Eq. (64) is void, for the expressions of $\mathbf{u}_{1(0)}$ and $\mathbf{u}_{2(0)}$ given above, as both $\lim_{r\to 0} u$ and $\lim_{r\to 0} v$ must be finite. Then,

$$\begin{bmatrix} \cos\theta_1 & \sin\theta_1 \\ \sin\theta_1 & -\cos\theta_1 \end{bmatrix} \begin{Bmatrix} p_1^I \\ p_1^{II} \end{Bmatrix} + \begin{bmatrix} \cos\theta_2 & \sin\theta_2 \\ \sin\theta_2 & -\cos\theta_2 \end{bmatrix} \begin{Bmatrix} p_2^I \\ p_2^{II} \end{Bmatrix} = \begin{Bmatrix} 0 \\ 0 \end{Bmatrix} \tag{69}$$

The simplest solution of this problem is obtained by electing the vector of force parameters $\begin{Bmatrix} p_x^* \\ p_y^* \end{Bmatrix}$ as the problem's primary unknowns (the superscript * standing for *fundamental solution*) and solving

$$\begin{Bmatrix} p_1^I \\ p_1^{II} \end{Bmatrix} = \begin{bmatrix} -\sin\theta_1 & \cos\theta_1 \\ +\cos\theta_1 & \sin\theta_1 \end{bmatrix} \begin{Bmatrix} p_x^* \\ p_y^* \end{Bmatrix}, \qquad \begin{Bmatrix} p_2^I \\ p_2^{II} \end{Bmatrix} = -\begin{bmatrix} -\sin\theta_2 & \cos\theta_2 \\ +\cos\theta_2 & \sin\theta_2 \end{bmatrix} \begin{Bmatrix} p_x^* \\ p_y^* \end{Bmatrix} \tag{70}$$

or

$$\mathbf{p}_1 = \mathbf{M}_1 \mathbf{p}^*, \qquad \mathbf{p}_2 = -\mathbf{M}_2 \mathbf{p}^* \tag{71}$$

The physical meaning of $\mathbf{p}^* \equiv \begin{Bmatrix} p_x^* \\ p_y^* \end{Bmatrix}$ becomes evident in the particularization of Eqs. (91) and (92) and also in comparison with the initially suggested Westergaard expressions for stress modes I and II [Mamani (2011)].

6.5 General displacement and stress expressions

One obtains from Eqs. (64) and (71) the displacement expression at a point (x,y):

$$\mathbf{u} = \left(\mathbf{T}_1^{\mathrm{T}} \mathbf{u}_{1(0)} \mathbf{M}_1 - \mathbf{T}_2^{\mathrm{T}} \mathbf{u}_{2(0)} \mathbf{M}_2\right) \mathbf{p}^* \tag{72}$$

The matrix product $\mathbf{T}_1^{\mathrm{T}} \mathbf{u}_{1(0)} \mathbf{M}_1$ that refers to the semicrack 1 may be explicitly expressed from Eqs. (52), (58), (62) and (70) as the sum of matrices of constants times the real and imaginary parts of the potential function derivatives, with similar procedure for the semicrack 2:

$$\mathbf{T}_1^{\mathrm{T}} \mathbf{u}_{1(0)} \mathbf{M}_1 = \mathbf{U}_{\mathrm{Im}\Phi_1} \mathrm{Im}\,\Phi_1 + \mathbf{U}_{\mathrm{Re}\Phi_1} \mathrm{Re}\,\Phi_1 + \mathbf{U}_{\mathrm{Im}\Phi_1'} \left(y_1 \mathrm{Im}\Phi_1'\right) + \mathbf{U}_{\mathrm{Re}\Phi_1'} \left(y_1 \mathrm{Re}\Phi_1'\right) \tag{73}$$

where

$$\mathbf{U}_{\mathrm{Im}\Phi_1} = \frac{2(1-\nu^2)}{E} \begin{bmatrix} 1 & 0 \\ 0 & 1 \end{bmatrix}, \quad \mathbf{U}_{\mathrm{Re}\Phi_1} = \frac{(1+\nu)(1-2\nu)}{E} \begin{bmatrix} 0 & 1 \\ -1 & 0 \end{bmatrix} \tag{74}$$

$$\mathbf{U}_{\mathrm{Im}\Phi_1'} = \frac{1+\nu}{Ea_1} \begin{bmatrix} \sin 2\theta_1 & -\cos 2\theta_1 \\ -\cos 2\theta_1 & -\sin 2\theta_1 \end{bmatrix}, \quad \mathbf{U}_{\mathrm{Re}\Phi_1'} = \frac{1+\nu}{Ea_1} \begin{bmatrix} \cos 2\theta_1 & \sin 2\theta_1 \\ \sin 2\theta_1 & -\cos 2\theta_1 \end{bmatrix} \tag{75}$$

Moreover, one obtains from Eqs. (63) and (71) the stress expression at a point (x,y):

$$\sigma = \left(\mathbf{R}_1 \sigma_{1(0)} \mathbf{M}_1 - \mathbf{R}_2 \sigma_{2(0)} \mathbf{M}_2\right) \mathbf{p}^* \tag{76}$$

The matrix product $\mathbf{R}_1 \sigma_{1(0)} \mathbf{M}_1$ that refers to the semicrack 1 may be explicitly expressed from Eqs. (53), (59), (63) and (70) as the sum of matrices of constants times the real and imaginary parts of the potential function derivatives:

$$\mathbf{R}_1 \sigma_{1(0)} \mathbf{M}_1 = \mathbf{S}_{\mathrm{Im}\Phi_1'} \mathrm{Im}\,\Phi_1' + \mathbf{S}_{\mathrm{Re}\Phi_1'} \mathrm{Re}\,\Phi_1' + \mathbf{S}_{\mathrm{Im}\Phi_1''} \left(y_1 \mathrm{Im}\Phi_1''\right) + \mathbf{S}_{\mathrm{Re}\Phi_1''} \left(y_1 \mathrm{Re}\Phi_1''\right)$$

(77)

where

$$\mathbf{S}_{\mathrm{Im}\Phi_1'} = \frac{2}{a_1}\begin{bmatrix} \cos^3\theta_1 & \sin\theta_1\cos^2\theta_1 \\ \sin^2\theta_1\cos\theta_1 & \sin^3\theta_1 \\ \sin\theta_1\cos^2\theta_1 & \sin^2\theta_1\cos\theta_1 \end{bmatrix} \tag{78}$$

$$\mathbf{S}_{\mathrm{Re}\Phi_1'} = \frac{1}{2a_1}\begin{bmatrix} -3\sin\theta_1 - \sin 3\theta_1 & 2\cos\theta_1\cos 2\theta_1 \\ 2\sin\theta_1\cos 2\theta_1 & 3\cos\theta_1 - \cos 3\theta_1 \\ 2\cos\theta_1\cos 2\theta_1 & 2\sin\theta_1\cos 2\theta_1 \end{bmatrix} \tag{79}$$

$$\mathbf{S}_{\mathrm{Im}\Phi_1''} = \frac{1}{a_1^2}\begin{bmatrix} \sin 3\theta_1 & -\cos 3\theta_1 \\ -\sin 3\theta_1 & \cos 3\theta_1 \\ -\cos 3\theta_1 & -\sin 3\theta_1 \end{bmatrix}, \quad \mathbf{S}_{\mathrm{Re}\Phi_1''} = \frac{1}{a_1^2}\begin{bmatrix} \cos 3\theta_1 & \sin 3\theta_1 \\ -\cos 3\theta_1 & -\sin 3\theta_1 \\ \sin 3\theta_1 & -\cos 3\theta_1 \end{bmatrix} \tag{80}$$

The matrix product $\mathbf{R}_2\sigma_{2(0)}\mathbf{M}_2$ for the semicrack 2 in Eq. (76) is obtained from Eqs. (77)–(80) by substituting the subscripts 2 for the subscripts 1.

For the purpose of computational implementation, the vectors of displacements $\mathbf{u}$ in Eq. (72) and of stresses σ in Eq. (76) can be compactly expressed as

$$\mathbf{u} = \left[\mathbf{U}_{cd1}\mathrm{Im}\Phi_{cd} + \mathbf{U}_{cd2}\mathrm{Re}\Phi_{cd}\right]\mathbf{p}^* \tag{81}$$

$$\sigma = \left[\mathbf{S}_{cd1}\mathrm{Im}\Phi'_{cd} + \mathbf{S}_{cd2}\mathrm{Re}\Phi'_{cd}\right]\mathbf{p}^* \tag{82}$$

Summation is implied for repeated indices. In these equations, $\mathbf{U}$ and $\mathbf{S}$ are $2\times 2\times 2$ arrays of matrix constants

$$\mathbf{U} = \begin{bmatrix} \begin{bmatrix} \mathbf{U}_{\mathrm{Im}\Phi_1} & \mathbf{U}_{\mathrm{Re}\Phi_1} \\ \mathbf{U}_{\mathrm{Im}\Phi_1'} & \mathbf{U}_{\mathrm{Re}\Phi_1'} \end{bmatrix} & \begin{bmatrix} -\mathbf{U}_{\mathrm{Im}\Phi_2} & -\mathbf{U}_{\mathrm{Re}\Phi_2} \\ -\mathbf{U}_{\mathrm{Im}\Phi_2'} & -\mathbf{U}_{\mathrm{Re}\Phi_2'} \end{bmatrix} \end{bmatrix} \tag{83}$$

$$\mathbf{S} = \begin{bmatrix} \begin{bmatrix} \mathbf{S}_{\mathrm{Im}\Phi_1'} & \mathbf{S}_{\mathrm{Re}\Phi_1'} \\ \mathbf{S}_{\mathrm{Im}\Phi_1''} & \mathbf{S}_{\mathrm{Re}\Phi_1''} \end{bmatrix} & \begin{bmatrix} -\mathbf{S}_{\mathrm{Im}\Phi_2'} & -\mathbf{S}_{\mathrm{Re}\Phi_2'} \\ -\mathbf{S}_{\mathrm{Im}\Phi_2''} & -\mathbf{S}_{\mathrm{Re}\Phi_2''} \end{bmatrix} \end{bmatrix} \tag{84}$$

A coefficient (c,d,j) refers with $c = 1,2$ to either semicrack, with $d = 1,2$ to the row number (d is related to *d*erivative) and with $j = 1,2$ to either the imaginary or real part of the potential functions Φ_1 or Φ_2. Each coefficient (c,d,j) of $\mathbf{U}$ is a 2×2 matrix given as in Eqs. (74)–(75) for the respective semicrack. Similarly, each coefficient (c,d,j) of $\mathbf{S}$ is a 3×2 matrix given as in Eqs. (78)–(80). The matrices $\Phi \equiv \Phi_{cd}$ and $\Phi' \equiv \Phi'_{cd}$ introduced in Eqs. (83) and (84) are defined as

$$\Phi = \begin{bmatrix} \Phi_1 & y_1\Phi_1' \\ \Phi_2 & y_2\Phi_2' \end{bmatrix}, \quad \Phi' = \begin{bmatrix} \Phi_1' & y_1\Phi_1'' \\ \Phi_2' & y_2\Phi_2'' \end{bmatrix} \tag{85}$$

6.6 Check that displacements and stresses are single valued when r tends to zero

According to the expressions of $\mathbf{u}_{1(0)}$ and $\mathbf{u}_{2(0)}$ given above, and using Eq. (70), one checks that both $\lim_{r\to 0} u$ and $\lim_{r\to 0} v$ are independent from the direction θ:

$$\lim_{r\to 0}\begin{Bmatrix} u \\ v \end{Bmatrix} = \frac{1+\nu}{\pi E}\cdot \begin{bmatrix} \dfrac{\sin 2\theta_1 - \sin 2\theta_2}{4} - (1-\nu)\Delta_{12} & \dfrac{1-2\nu}{2}\ln\dfrac{a_1}{a_2} + \dfrac{\cos 2\theta_4 - \cos 2\theta_1}{2} \\ -\dfrac{1-2\nu}{2}\ln\dfrac{a_1}{a_2} + \dfrac{\cos 2\theta_4 - \cos 2\theta_1}{2} & \dfrac{\sin 2\theta_2 - \sin 2\theta_1}{4} - (1-\nu)\Delta_{12} \end{bmatrix} \begin{Bmatrix} p_x^* \\ p_y^* \end{Bmatrix} \tag{86}$$

The term $\Delta_{12} = \theta_2 - \theta_1 \pm 2\pi$ in the above equation depends on whether $r = 0$ is approached from inside or outside the domain, as explained for the potential problem, which indicates a displacement jump along the crack faces. The relevant aspect of this equation is that both $\lim_{r\to 0} u$ and $\lim_{r\to 0} v$ are finite and single valued when $r = 0$ is approached from inside the domain.

Moreover, one obtains from Eq. (76), after some tedious manipulations,

$$\lim_{r\to 0}\begin{Bmatrix} \sigma_x \\ \sigma_y \\ \tau_{xy} \end{Bmatrix} = \begin{bmatrix} \dfrac{\cos\theta_1 + \cos 3\theta_1}{8a_1} - \dfrac{\cos\theta_2 + \cos 3\theta_2}{8a_2} & \dfrac{3\sin\theta_2 + \sin 3\theta_2}{8a_2} - \dfrac{3\sin\theta_1 + \sin 3\theta_1}{8a_1} \\ \dfrac{3\cos\theta_1 - \cos 3\theta_1}{8a_1} - \dfrac{3\cos\theta_2 - \cos 3\theta_2}{8a_2} & \dfrac{\sin\theta_2 - \sin 3\theta_2}{8a_2} - \dfrac{\sin\theta_1 + \sin 3\theta_1}{8a_1} \\ \dfrac{\sin 3\theta_1 - \sin\theta_1}{8a_1} - \dfrac{\sin 3\theta_2 - \sin\theta_2}{8a_2} & \dfrac{\cos\theta_1 + \cos 3\theta_1}{8a_1} - \dfrac{\cos\theta_2 + \cos 3\theta_2}{8a_2} \end{bmatrix} \begin{Bmatrix} p_x^* \\ p_y^* \end{Bmatrix} \tag{87}$$

which is finite and single valued.

6.7 Behavior of the traction forces along a crack surface

The traction forces

$$T_i = \sigma_{ji} n_j, \quad \text{or} \quad \begin{Bmatrix} T_x \\ T_y \end{Bmatrix} = \begin{bmatrix} n_x & 0 & n_y \\ 0 & n_y & n_x \end{bmatrix} \begin{Bmatrix} \sigma_x \\ \sigma_y \\ \tau_{xy} \end{Bmatrix} \quad \text{or} \quad \mathbf{t} = \mathbf{n}\sigma \tag{88}$$

are generically expressed, according to Eq. (76) and above, as

$$\mathbf{t} = \mathbf{n}\left(\mathbf{R}_1 \sigma_{1(0)} \mathbf{M}_1 - \mathbf{R}_2 \sigma_{2(0)} \mathbf{M}_2\right) \mathbf{p}^* \tag{89}$$

Along the crack surface $\theta = \theta_1$, where the projections of the outward unit normal $\vec{n}$ along the direction θ_1 are $n_x = \sin\theta_1$ and $n_y = -\cos\theta_1$, one obtains

$$\mathbf{n}|_{\theta=\theta_1}\mathbf{R}_1\boldsymbol{\sigma}_{1(0)}\mathbf{M}_1 = -\frac{\mathrm{Re}\,\Phi_1'}{a_1}\begin{bmatrix}1 & 0\\ 0 & 1\end{bmatrix} + \frac{y_1}{a_1^2}\begin{bmatrix}\cos 2\theta_1 & \sin 2\theta_1\\ \sin 2\theta_1 & -\cos 2\theta_1\end{bmatrix}\begin{bmatrix}\mathrm{Im}\,\Phi_1'' & \mathrm{Re}\,\Phi_1''\\ \mathrm{Re}\,\Phi_1'' & -\mathrm{Im}\,\Phi_1''\end{bmatrix} \tag{90}$$

which enables assessing the singularity behavior of the stresses along a crack surface. The above equation shows only the contribution of the semicrack 1 to the total stress expression of Eq. (89). There are actually no singularities at $r = 0$, according to Eq. (87). Since $y_1 = 0$ along the crack surface $\theta = \theta_1$, according to Eq. (50), one can write from Eq. (90) that, simply,

$$\mathbf{n}|_{\theta=\theta_1}\mathbf{R}_1\boldsymbol{\sigma}_{1(0)}\mathbf{M}_1 = -\frac{\mathrm{Re}\,\Phi_1'}{a_1}\begin{bmatrix}1 & 0\\ 0 & 1\end{bmatrix} \quad \text{along the crack surface } \theta = \theta_1 \tag{91}$$

and, similarly,

$$\mathbf{n}|_{\theta=\theta_2}\mathbf{R}_2\boldsymbol{\sigma}_{2(0)}\mathbf{M}_2 = -\frac{\mathrm{Re}\,\Phi_2'}{a_2}\begin{bmatrix}1 & 0\\ 0 & 1\end{bmatrix} \quad \text{along the crack surface } \theta = \theta_2 \tag{92}$$

In either case there is only a logarithmic singularity at $r = 0$ due to $\mathrm{Re}\,\Phi'$, as in the case of the potential problem (Section 5.1.2). The latter two expressions justify the particular choice of the parameters $\begin{Bmatrix}p_x^*\\ p_y^*\end{Bmatrix}$ in Eq. (71) [Mamani (2011)].

6.8 *Numerical integration of the double-layer potential matrix* **H** *for elasticity problems*

The general expression of the double-layer potential matrix **H** for elasticity problems is

$$\mathbf{H} \equiv H_{mn} = \int_\Gamma \sigma_{jim} n_j u_{in}\,\mathrm{d}\Gamma \tag{93}$$

where m denotes one of the directions of application of the nominal crack forces $\mathbf{p}^* \equiv \begin{Bmatrix}p_x^*\\ p_y^*\end{Bmatrix}$, defined in Eq. (70), at the node k and n is the direction (x or y) of application of a unit displacement, which is linearly interpolated. The procedure shown for the potential problem in Section 5.2 was much simpler than the present case, as now there is a 2×2 matrix associated to each nodal point. The potential problem algorithm was also simpler because only integrations related to Φ_1' had to be carried out, whereas the elasticity problem requires dealing with Φ_1'' as well.

However, the stress representation of Eq. (77) leads to a procedure that is logically exactly the same one of the potential problem. In fact, one can carry out all integrations related to the complex scalars Φ'_1, Φ''_1, Φ'_2 and Φ''_2 and build the final matrix results afterwards, in terms of the matrices of constants of Eq. (77), which are geometric characteristics of the semicracks adjacent to a node k, pre-multiplied by the matrix $\mathbf{n}$ defined in Eq. (88).

The following Section consists in an algorithm for the numerical evaluation of Eq. (93) that is logically the same one outlined in Section 5.2 for potential problems. The additional computational requirements for elasticity problems are related to the data preparation – the matrices of constants of Eq. (77) – and the final representation of the 2×2 matrix of results, according to Eq. (89). In order to have an algorithm that is self-contained, several features presented in Section 5.2.1 are reproduced here.

6.8.1 Algorithm for the numerical integration of $\mathbf{H}$

Let nn be the total number of nodes of a discretized model, which coincides with the total number of discretized boundary segments. A body of any topology, with reentrant corners, holes and, after a slight modification of the basic code, also generally curved, internal cracks, can be simulated.

Define the matrices of potential functions

$$\Phi' = \begin{bmatrix} \Phi'_1 & y_1\Phi''_1 \\ \Phi'_2 & y_2\Phi''_2 \end{bmatrix}, \quad \Phi'_{ln} = \begin{bmatrix} \Phi'_1 & y_1\Phi''_1 \\ \Phi'_2 & y_2\Phi''_2 \end{bmatrix}_{ln}, \quad \Phi'_{reg} = \begin{bmatrix} \Phi'_1 & y_1\Phi''_1 \\ \Phi'_2 & y_2\Phi''_2 \end{bmatrix}_{reg} \tag{94}$$

The matrix Φ' was already introduced on the right of Eq. (85). The subscripts $()_{ln}$ and $()_{reg}$ above indicate that the functions in the matrix coefficients are the ones defined in Eqs. (A.6) and (A.7), for the logarithmic singularity, and (A.18) and (A.19), for the $\sqrt{1/\xi}$ singularity. Also, define the matrix $\mathbf{N}$ of shape functions

$$\mathbf{N} = \begin{bmatrix} N_i & N_j \end{bmatrix} \equiv \begin{bmatrix} 1-\xi & \xi \end{bmatrix} \tag{95}$$

Moreover, define the $(2 \times nn) \times (2 \times nn)$ matrix $\mathbf{H}$ with all coefficients initially set as zero.

For the purpose of having the following algorithm as ready as possible for code writing, the coefficients of all matrices are referred to in brackets whereas the primary variable is given in parentheses, such as $\Phi'(\xi)[c,d]$, where $c,d = 1,2$ for the first matrix in Eq. (94).

External loop for the *source cracks* **with** k **varying from 1 to** nn**.** Determine the adjacent nodes k^- and k^+, for the nodes numbered counterclockwise. Next, obtain

$\cos\theta_1$, $\sin\theta_1$, $\cos\theta_2$, $\sin\theta_2$, T_1 and T_2, according to Section 4 and define the array of constants $\mathbf{S}$ of Eq. (84), here repeated for clarity:

$$\mathbf{S} = \begin{bmatrix} \begin{bmatrix} \mathbf{S}_{\mathrm{Im}\Phi_1'} & \mathbf{S}_{\mathrm{Re}\Phi_1'} \\ \mathbf{S}_{\mathrm{Im}\Phi_1''} & \mathbf{S}_{\mathrm{Re}\Phi_1''} \end{bmatrix} & \begin{bmatrix} -\mathbf{S}_{\mathrm{Im}\Phi_2'} & -\mathbf{S}_{\mathrm{Re}\Phi_2'} \\ -\mathbf{S}_{\mathrm{Im}\Phi_2''} & -\mathbf{S}_{\mathrm{Re}\Phi_2''} \end{bmatrix} \end{bmatrix}$$

Internal loop for the *integration segments* **with** i **varying from 1 to** nn**.** Determine the subsequent node j, as integration will be carried out along the segment $\overline{ij}$.

Evaluate $x(\xi)$ and $y(\xi)$ along the segment $\overline{ij}$ as well as the derivatives $dx/d\xi$ and $dy/d\xi$ and the Jacobian $|J|$. Observe that, in Eq. (93), $n_x \mathrm{d}\Gamma = dy$ and $n_y \mathrm{d}\Gamma = -dx$. Next, evaluate $Z_1(\xi)$ and $Z_2(\xi)$, according to Eq. (17).

Carry out the numerical evaluation of the $2 \times 2 \times 2$ complex array $\mathbf{h}$ in the following *logical if* structure using the procedures $lnproc()$ and $sqrtproc()$ given in the Appendix. In the loops to be presented, $c = 1,2$ refers to either semicrack 1 or 2, $d = 1,2$ refers to either derivative order 1 or 2 of $\Phi(Z)$, and $n = 1,2$ refers to either extremity i or j of a segment.

If $i = k$, then there is an embedded logarithmic singularity at the extremity $\xi = 0$ of the segment $\overline{ij}$ caused by the semicracks along both segments $\overline{kk^+}$ and $\overline{k^-k}$: case (a) of Fig. 5.

For c, d and n varying from 1 to 2 in three nested loops,

Define $f = \Phi'(\xi)[c,d]\mathbf{N}(\xi)[n]$, $f_{ln} = \Phi'_{ln}(\xi)[c,d]\mathbf{N}(\xi)[n]$, $f_{reg} = f - f_{ln}\ln\xi$ and obtain $\mathbf{h}[n,c,d] = lnproc()$.

End of the nested loops with c,d,n.

Else if $j = k$, then there is an embedded logarithmic singularity at the extremity $\xi = 1$ of the segment $\overline{ij}$ caused by the semicracks along both segments $\overline{kk^+}$ and $\overline{k^-k}$: case (b) of Fig. 5.

For c, d and n varying from 1 to 2 in three nested loops,

Define $f = \Phi'(1-\xi)[c,d]\mathbf{N}(1-\xi)[n]$, $f_{ln} = \Phi'_{ln}(1-\xi)[c,d]\mathbf{N}(1-\xi)[n]$, $f_{reg} = f - f_{ln}\ln\xi$ and obtain $\mathbf{h}[n,c,d] = lnproc()$.

End of the nested loops with c,d,n.

Else if $i = k^+$, then there is a square-root singularity at the extremity $\xi = 0$ of the segment $\overline{ij}$ caused by semicrack 1 along the segment $\overline{kk^+}$: case (c) of Fig. 5. There is no singularity associated with the semicrack 2.

For d and n varying from 1 to 2 in two nested loops,

Define $f = \Phi'(\xi)[1,d]\mathbf{N}(\xi)[n]$, $f_{reg} = \Phi'_{reg}(\xi)[1,d]\mathbf{N}(\xi)[n]$, $f_{sqrt} = (f - f_{reg})\sqrt{\xi}$ and obtain $\mathbf{h}[n,1,d] = sqrtproc()$.

Define $f = \Phi'(\xi)[2,d]\mathbf{N}(\xi)[n]$ and carry out the Gauss-Legendre quadrature $\mathbf{h}[n,2,d] = \sum_{i_g=1}^{n_g} f(\xi_g[i_g])w_g[i_g]$.

End of the nested loops with d,n.

Else if $j = k^-$, then there is a square-root singularity at the extremity $\xi = 1$ of the segment $\overline{ij}$ caused by semicrack 2 along the segment $\overline{k^-k}$: case (d) of Fig. 5. There is no singularity associated with the semicrack 1.

For d and n varying from 1 to 2 in two nested loops,

Define $f = \Phi'(1-\xi)[2,d]\mathbf{N}(1-\xi)[n]$, $f_{reg} = \Phi'_{reg}(1-\xi)[2,d]\mathbf{N}(1-\xi)[n]$, $f_{sqrt} = (f - f_{reg})\sqrt{\xi}$ and obtain $\mathbf{h}[n,2,d] = sqrtproc()$.

Define $f = \Phi'(\xi)[1,d]\mathbf{N}(\xi)[n]$ and carry out the Gauss-Legendre quadrature $\mathbf{h}[n,1,d] = \sum_{i_g=1}^{n_g} f(\xi_g[i_g])w_g[i_g]$.

End of the nested loops with d,n.

Else there is no singularity: case (e) of Fig. 5.

For c, d and n varying from 1 to 2 in three nested loops,

Define $f = \Phi'(\xi)[c,d]\mathbf{N}(\xi)[n]$ and carry out the Gauss-Legendre quadrature $\mathbf{h}[n,c,d] = \sum_{i_g=1}^{n_g} f(\xi_g[i_g])w_g[i_g]$.

End of the nested loops with c,d,n.

End if End of the *structured logical if*.

Define the matrix of boundary unit projections of Eq. (88) referred to the segment $\overline{ij}$, here repeated for convenience,

$$\mathbf{n} = \begin{bmatrix} n_x & 0 & n_y \\ 0 & n_y & n_x \end{bmatrix}$$

The 2×2 submatrix $\mathbf{H}_{sub}$ of the matrix $\mathbf{H}$ in Eq. (93) is obtained in the following loop, according to Eq. (89), for nodes i and j given in the array $\mathbf{i} \equiv [i,j]$, .

Loop for extremities i and j, with n varying from 1 to 2

$$\mathbf{H}_{sub} = \left[\sum_{c=1}^{2} \sum_{d=1}^{2} \mathbf{C}[c,d,1]\,\mathrm{Im}(\mathbf{h}[n,c,d]) + \mathbf{C}[c,d,2]\,\mathrm{Re}(\mathbf{h}[n,c,d]) \right]^{\mathrm{T}} \mathbf{n}^{\mathrm{T}} \tag{96}$$

The matrix $\mathbf{H}$, whose coefficients may already have contribution from a preceding integration over an adjacent segment, is obtained from $\mathbf{H}_{sub}$ as

$$\mathbf{H}[2(k-1)+\ell, 2(\mathbf{i}[n]-1)+m] = \mathbf{H}[2(k-1)+\ell, 2(\mathbf{i}[n]-1)+m] + \mathbf{H}_{sub}[\ell, m], \;\; \ell, m = 1,2 \tag{97}$$

End of loops with control variables n, i, k.

7 Numerical examples

7.1 Application to a potential problem

A logarithmic potential source $\Phi = \ln\sqrt{(x+10)^2+(y-25)^2}/(2\pi)$ is applied at node **F** of an unbounded two-dimensional continuum, as illustrated in Figure 6. The depicted irregular figure is cut out and the potential and gradients evaluated along the boundaries are applied, thus creating a problem (for the Laplace equation) of simple, known analytical solution. However, the reentrant corner and the internal hole of the figure pose some topological difficulties to the numerical simulation. The figure is composed of a total of 104 nodes and linear segments, which are equally spaced between the indicated corner nodes, whose coordinates are given in Tab. 1. A series of 51 points along the line segment $\overline{AB}$ are also generated for the representation of some numerical results in the domain.

Table 1: Cartesian Coordinates of the nodes that constitute Fig. 6.

Node	1	17	27	50	69	87	93	99	A	B	F
x	0	10	20	15	0	10	11	12	5	15	-10
y	0	15	10	35	20	20	21	20	20	18	25

The simplest problem that can be solved in this example is for Neumann boundary conditions, when only the matrix $\mathbf{H}$ of Eq. (8), as developed in Eq. (42) for potential problems, needs be evaluated [Dumont and Mamani (2011b)]. Although $\mathbf{H}$ is a singular matrix for a bounded domain, the equivalent nodal gradients $\mathbf{p}$ of Eq. (8) are in balance and the posed linear algebra problem admits of just one solution $\mathbf{p}^*$, to be obtained in the frame of generalized inverse matrices [Dumont (1989); Dumont and Lopes (2003); Mamani (2011)]. Once $\mathbf{p}^*$ is evaluated, gradients and potentials can be obtained according to Eqs. (4) and (5). Figure 7 shows on the left both analytical and numerical values of the potential, as obtained along the line segment $\overline{AB}$. Since this is a Neumann problem, a constant potential was added to the

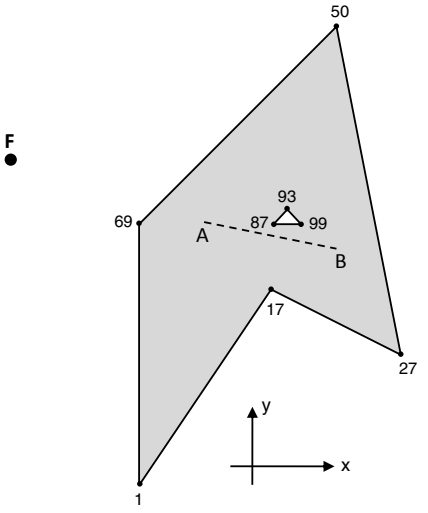

Figure 6: Cut-out model for the numerical modeling of a multiply connected body.

numerical results in order that both analytical and numerical values best coincide. Analytical and numerical values of gradients are also shown in Fig. 7.

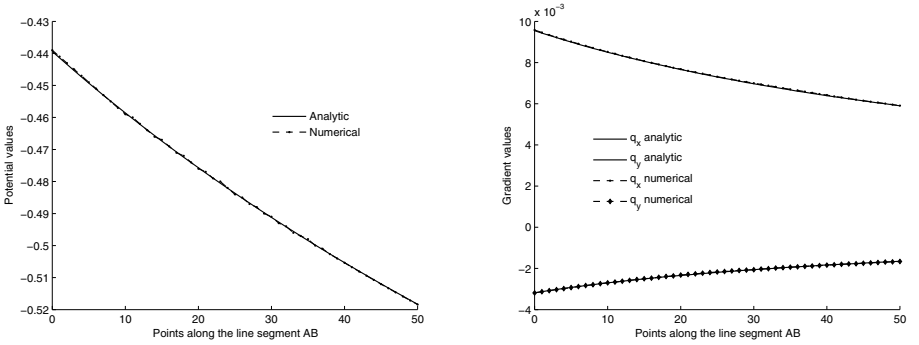

Figure 7: Comparison of some analytical and numerical results for the example of Fig. 6.

7.2 Application to an elasticity problem

The same irregular figure illustrated in Fig. 6 is used for the numerical simulation of a two-dimensional elasticity problem (Poisson's ratio equal to 0.3), for a horizontal point force of unit intensity applied at a node of coordinates $(-10, 25)$.

Displacements and traction forces due to the point force, as measured along the drawn boundaries, are applied to create a problem of known analytical solution that, due to the lack of convexity of the cut-out domain, is difficult to solve numerically [Dumont and Mamani (2011a)]. In this example, the figure is composed of a total of 170 nodes and linear segments that are equally spaced between the indicated corner nodes, corresponding to the node numbering given in the fourth row of Tab. 2.

The graphics of Fig. 8 show both analytical and numerical stress values obtained along 51 points of the same line segment $\overline{AB}$ of the previous example (the values of σ_{xx} are multiplied by -1). Accuracy of results obtained in a formulation that uses Kelvin fundamental solution is almost matched, in this particular numerical example [Dumont and Mamani (2011b)]. However, the boundary layer effect is larger in the case of fundamental solutions defined in terms of generalized Westergaard functions. In fact, one observes in the graphics that the simulated hole in the figure disturbs the numerical values of σ_{xy} and σ_{yy}, which slightly undulate about the analytical results. This is expected, as the gradient singularity $\sqrt{1/r}$ of the Westergaard function is less localized than the singularity $1/r$ given by Kelvin's fundamental solution. In spite of that, good accuracy can be still achieved after some post-processing of the results for points close to or on the boundary, as done for the case of Kelvin fundamental solutions [Dumont and Lopes (2003); Dumont (2011)].

7.3 A convergence study

A comparative convergence study of the numerical simulations of the potential and elasticity problems of the previous sections is given in Fig. 9, for numerical discretizations with total numbers 30, 58, 114, 170 and 227 of nodes shown in the abscissas. (The simulation with 227 nodes was run only for elasticity.) The respective corner nodes of Fig. 6 are given in Tab. 2.

The graphics display, for each performed numerical simulation, the Euclidean error

Table 2: Corner numbers of the various mesh discretizations of Fig. 6.

30	1	5	8	14	19	24	26	28
58	1	9	14	26	36	45	49	53
114	1	17	27	50	69	87	95	103
170	1	25	40	74	103	130	142	154
227	1	33	53	99	137	173	189	205

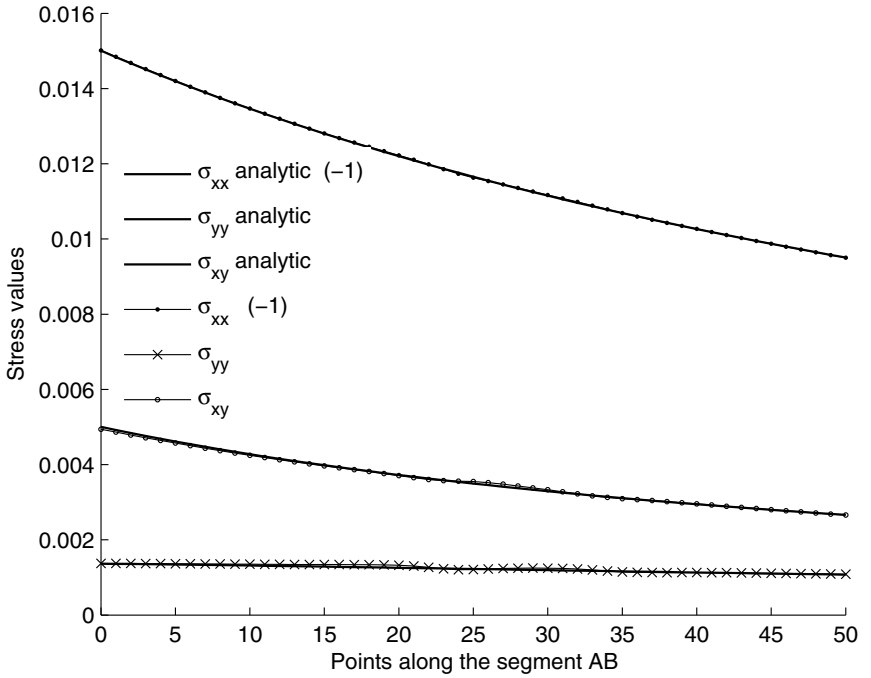

Figure 8: Comparison of analytical and numerical stress results along the line segment $\overline{AB}$ of Fig. 6, for a horizontal point force at $(-10,25)$.

norm of gradients or stresses evaluated according to the formula

$$\varepsilon = \sqrt{\sum_{i=1}^{51} \left(v_a[i] - v_n[i]\right)^2 \Big/ \sum_{i=1}^{51} v_a[i]^2} \tag{98}$$

where $v_n[i]$ and $v_a[i]$ stand for the numerical and analytical values obtained at any of the 51 points along the line segment $\overline{AB}$. The results in Fig. 9 are indicated for Kelvin (K) and Westergaard (W) fundamental solutions. The results for the conventional, collocation boundary element method (Kelvin fundamental solutions) converge faster, as expected. However, a neat convergence pattern could also be shown for the formulation proposed in terms of Westergaard stress functions.

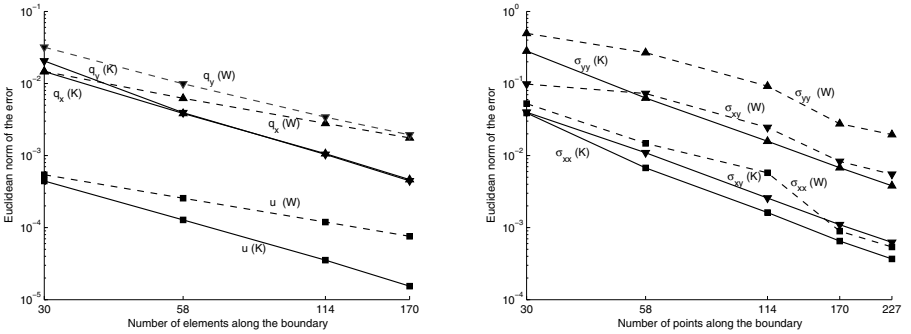

Figure 9: Comparative convergence study of implementations for the irregularly-shaped figure using Kelvin and Westergaard fundamental solutions for potential (on the left) and elasticity problems.

Conclusions

The ultimate goal of the present research project is to obtain a formulation for the modeling of cracks, as illustrated in Fig. 4, which can also be applied to holes and notches and leads to a straightforward evaluation of stress intensity and concentration factors, as a generalization of the developments of Dumont and Lopes (2003). The scheme of the curved crack in Fig. 4 is topologically a hole with n nodes and segments, similar to the one with nodes 87…104 of Fig. 6, except that, after evaluation of the problem's matrices and vectors, rows and columns referring to nodes assigned as 1, $n+2$ and $n+3$ in Fig. 4 are removed from the equation systems.

This paper focuses on the conceptual layout of fundamental solutions that are generalizations of the stress functions proposed by Westergaard for mode I and mode II deformation problems. Completeness of the formulation in terms of the Kolosov-Muskhelishvili potentials [Sadd (2005)] is guaranteed for almost all domain topology and boundary conditions, provided that some spectral properties of the resultant matrices are adequately taken into account [Dumont and Mamani (2011b); Dumont (2011)]. As proposed, the formulation would not work, for instance, for a point force applied inside the hole of Fig. 6.

However, the present fundamental solution is not meant as a surrogate for Kelvin's formulation and it may not be worth attempting to arrive at a complete generalization. The numerical examples above were shown with the purpose of validating the theoretical developments. The best numerical simulation of problems of fracture mechanics seems to be achievable by conveniently combining Kelvin fundamental solutions and the proposed generalized stress functions [Dumont and Lopes (2003);

Dumont and Mamani (2011b)].

The evaluation of stress intensity factors in fracture mechanics problems can be carried out easily and more accurately in the present context than using any existing finite element or boundary element codes. The specific issues of this subject are dealt with in a forthcoming paper.

Acknowledgement: This project was supported by the Brazilian agencies CAPES, CNPq and FAPERJ.

References

Brebbia, C. A.; Telles, J. F. C.; Wrobel, L. C. (1984): *Boundary Element Techniques*. Springer-Verlag, Berlin.

Crouch, S. L.; Starfield, A. M. (1983): *Boundary Element Methods in Solid Mechanics*. George Allen & Unwin, London.

Dumont, N. A. (1989): The hybrid boundary element method: an alliance between mechanical consistency and simplicity. *Applied Mechanics Reviews*, vol. 42, no. 11, pp. S54–S63.

Dumont, N. A. (2003): Variationally-based, hybrid boundary element methods. *Computer Assisted Mechanics and Engineering Sciences (CAMES)*, vol. 10, pp. 407–430.

Dumont, N. A. (2008): Dislocation-based hybrid boundary element method. Draft paper, 2008.

Dumont, N. A. (2011): The hybrid boundary element method – fundamentals (*to be submitted*). *Engineering Analysis with Boundary Elements*.

Dumont, N. A.; Chaves, R. A. P.; Paulino, G. H. (2004): The hybrid boundary element method applied to problems of potential of functionally graded materials. *International Journal of Computational Engineering Science (IJCES)*, vol. 5, pp. 863–891.

Dumont, N. A.; de Oliveira, R. (2001): From frequency-dependent mass and stiffness matrices to the dynamic response of elastic systems. *International Journal of Solids and Structures*, vol. 38, no. 10-13, pp. 1813–1830.

Dumont, N. A.; Huamán, D. (2009): Hybrid finite/boundary element formulation for strain gradient elasticity problems. In Sapountzakis, E. J.; Aliabadi, M. H.(Eds): *Advances in Boundary element Techniques X*, pp. 295–300, Athens, Greece. EC, Ltd, UK.

Dumont, N. A.; Lopes, A. A. O. (2003): On the explicit evaluation of stress intensity factors in the hybrid boundary element method. *Fatigue & Fracture of Engineering Materials & Structures*, vol. 26, pp. 151–165.

Dumont, N. A.; Mamani, E. Y. (2011): Use of generalized Westergaard stress functions as fundamental solutions. In Albuquerque, E. L.; Aliabadi, M. H.(Eds): *Advances in Boundary element Techniques XII*, pp. 143–157, Brasilia, Brazil. EC, Ltd., UK.

Dumont, N. A.; Mamani, E. Y. (2011): A variational boundary element method based on generalized Westergaard stress functions. In E. A. Fancello, P. T. R. M.; Alves, M.(Eds): *Solids Mechanics in Brazil 2011*, pp. 143–157, Florianopolis, Brazil. Brazilian Society of Mechanical Sciences and Engineering.

Lopes, A. A. O. (2002): *Evaluation of stress intensity factors with the hybrid boundary element method (in Portuguese).* PhD thesis, Pontifical Catholic University of Rio de Janeiro, Brazil, 2002.

Mamani, E. Y. (2011): The hybrid boundary element method based on generalized Westergaard stress functions (in Portuguese). Master's thesis, Pontifical Catholic University of Rio de Janeiro, 2011.

Pian, T. H. H. (1964): Derivation of element stiffness matrices by assumed stress distribution. *AIAA Journal*, vol. 2, pp. 1333–1336.

Sadd, M. H. (2005): *Elasticity Theory, Applications, and Numerics*. Elsevier, Burlington, USA.

Tada, H.; Ernst, H.; Paris, P. (1993): Westergaard stress functions for displacement-prescribed crack problems - I. *International Journal of Fracture*, vol. 61, pp. 39–53.

Tada, H.; Ernst, H.; Paris, P. (1994): Westergaard stress functions for displacement-prescribed crack problems - II. *International Journal of Fracture*, vol. 67, pp. 151–167.

Appendix A: Numerical integration issues for singularities at the extremities of a segment

The following developments are expansions about the extremities of either segment 1 or 2. For simplicity, the subscript is suppressed in this Section.

A.1 Singularity of the potential function $\Phi(Z)$ and its derivatives about $Z=0$

The expansion of $\Phi(Z)$ and its derivatives about the origin follows from Eqs. (16), (21) and (25) as

$$\Phi(Z) \approx \left(\frac{1}{2\pi}-\frac{Z^2}{4\pi}-\frac{Z^4}{16\pi}+\cdots\right)\left(-\ln\frac{Z}{2}+i\pi\,\mathrm{signal}(Z)\right)-\frac{1}{2\pi}-\frac{Z}{4}-\frac{Z^2}{8\pi}+\frac{Z^4}{64\pi}+\cdots \tag{A.1}$$

$$\Phi'(Z) = \left(\frac{Z}{2\pi}+\frac{Z^3}{4\pi}+\frac{3Z^5}{16\pi}+\cdots\right)\left(\ln\frac{Z}{2}-i\pi\,\mathrm{signal}(Z)\right)-\frac{1}{2\pi Z}-\frac{1}{4}+\frac{Z^3}{8\pi}+\frac{7Z^5}{64\pi}+\cdots \tag{A.2}$$

$$\Phi''(Z) = \left(\frac{1}{2\pi}+\frac{3Z^2}{4\pi}+\frac{15Z^4}{16\pi}+\cdots\right)\left(\ln\frac{Z}{2}-i\pi\,\mathrm{signal}(Z)\right)+\frac{1}{2\pi Z^2}+\frac{1}{2\pi}+\frac{5Z^2}{8\pi}+\frac{47Z^4}{64\pi}+\cdots \tag{A.3}$$

where the function

$$\mathrm{signal}(Z) = \mathrm{csgn}\left(\frac{\left(1+\sqrt{1-Z^2}\right)i}{Z}\right) \tag{A.4}$$

which eventually contributes to a jump of the potential function and its derivatives, can be simply overlooked in the numerical implementations, as it will be implicit in the *regular* part of the series developments, according to the following Eqs. (A.5)-(A.8). The jump issues of $\Phi(Z)$ and its derivatives were dealt with for potential problems in Section 5.1 and for elasticity in Sections 6.6 and 6.7. As seen in the theoretical developments, the $\ln Z$, $1/Z$ and $1/Z^2$ singularities cancel out when two segments are taken into account. Although there is no actual ln singularity in the expression of $\Phi'(Z)$, the terms affected by $\ln Z$ deserve attention in the numerical integration, as a Gauss-Legendre quadrature would lead to inaccuracies. The second derivative Φ'' of the potential function is required only for elasticity problems and is always multiplied by $y_1 = r\sin(\theta-\theta_1)$. Then, the actual singularity would be $1/Z$, which cancels out when two segments are taken into account, as outlined in Section 6.5.

One writes Eqs. (A.1), (A.2) and (A.3) for the developments about $Z=0$ as

$$\Phi(Z) \approx \Phi_{ln}(Z)\ln\xi + \Phi_{reg}(Z) \tag{A.5}$$

$$\Phi'(Z) \approx \Phi'_{ln}(Z)\ln\xi + \Phi'_{reg}(Z) \tag{A.6}$$

$$\Phi''(Z) \approx \Phi''_{ln}(Z)\ln\xi + \Phi''_{reg}(Z) \tag{A.7}$$

where $\Phi_{ln}(Z)$, $\Phi'_{ln}(Z)$ and $\Phi''_{ln}(Z)$ are the terms in brackets on the left of Eqs. (A.1), (A.2) and (A.3), and evaluates $\Phi_{reg}(Z)$, $\Phi'_{reg}(Z)$ and $\Phi''_{reg}(Z)$ by subtractions from the complete, non-expanded expressions of Eqs. (16), (21) and (25), as

$$\Phi_{reg}(Z) = \Phi(Z) - \Phi_{ln}(Z)\ln\xi \tag{A.8}$$

in the case of $\Phi(Z)$ and similarly for its derivatives. This subtraction is simple and numerically effective, as a quadrature algorithm will never make use of the abscissa $\xi = 0$.

In the developments just outlined, $\Phi_{reg}(Z)$ and its derivatives are the *regular* part of the expansions about the origin, but can be hardly approached by a low-order polynomial expression, for Z close do zero. A numerical integration algorithm for a general improper integral with logarithmic singularity is described in the next Section. The developments are directly applicable to the case of the logarithmic singularity $\ln(1-\xi)$ by just making a coordinate transformation from ξ to $1-\xi$.

A.2 Quadrature of a function with logarithmic singularity with the use of subintervals

The following algorithm carries out the numerical quadrature

$$F = \int_0^1 f(\xi)\,\mathrm{d}\xi \equiv \int_0^1 \left(f_{ln}(\xi)\ln\xi + f_{reg}(\xi)\right)\mathrm{d}\xi \tag{A.9}$$

where both $f_{ln}(\xi)$ and $f_{reg}(\xi)$ have no embedded singularities but cannot be approximated by a low-order polynomial about $\xi = 0$. However, it is assumed that the function $f(\xi)$ can be approximated by a low-order polynomial about $\xi = 1$. As proposed, one is in principle dealing with an improper integral. However, this routine should be applied also in the case of $\lim_{\xi\to 0} f_{ln}(\xi) = 0$.

The interval $[0,1]$ is split into n_Δ subintervals of increasing magnitude counting from $\xi = 0$, such that $\Delta\xi_i = \alpha\Delta\xi_{i-1}$, for $i = 2..n_\Delta$. A special quadrature of $f_{ln}(\xi)\ln\xi$ is carried out in the interval $[0,\Delta\xi_1]$ and a Gauss-Legendre quadrature evaluates the remaining parts of the integral in Eq. (A.9) along the successive, increasingly larger subintervals.

Input data. The input data for the algorithm are:

- Functions $f(\xi), f_{ln}(\xi)$ and $f_{reg}(\xi)$.
- Number of subintervals n_Δ (recommended value is $n_\Delta = 4$).
- Subinterval amplification factor α (recommended value is $\alpha = 2$).

- Data for the logarithm quadrature: number of abscissas n_l, abscissas $\xi_l[\,]$ and weights $w_l[\,]$ (recommended value is $n_l = 5$).
- Data for the Gauss-Legendre quadrature: number of abscissas n_g, abscissas $\xi_g[\,]$ and weights $w_g[\,]$ (recommended value is $n_g = 5$).

Ouput. The output of the algorithm is the numerical value F of the integral in Eq. (A.9).

Algorithm. Define the length and start point of the first interval:

$$\Delta\xi = \frac{\alpha - 1}{\alpha_\Delta^n - 1}; \quad \xi_i = 0 \tag{A.10}$$

- Evaluate $\int_0^{\Delta\xi} f(\xi)\,\mathrm{d}\xi$ numerically along the first interval by adequately splitting the integrand into regular and improper parts (and also taking care of interval normalization):

$$F = \Delta\xi \sum_{i=1}^{n_g} \left(f_{reg}\left(\xi_g[i]\Delta\xi\right) + f_{ln}\left(\xi_g[i]\Delta\xi\right) \ln\Delta\xi \right) w_g[i] + \Delta\xi \sum_{i=1}^{n_l} f_{ln}\left(\xi_l[i]\Delta\xi\right) w_l[i] \tag{A.11}$$

  In this equation, $f_{reg}(\xi) = f(\xi) - f_{ln}(\xi)\ln\xi$.

- For a loop with $n_\Delta - 1$ repetitions, successively update the values of Eq. (A.10) as

$$\xi_i = \xi_i + \Delta\xi; \quad \Delta\xi = \alpha\,\Delta\xi \tag{A.12}$$

  and carry out the numerical evaluation of $\int_{\xi_i}^{\xi_i+\Delta\xi} f(\xi)\,\mathrm{d}\xi$:

$$F = F + \Delta\xi \sum_{i=1}^{ng} f\left(\xi_i + \xi_g[i]\Delta\xi\right) w_g[i] \tag{A.13}$$

A.3 Singularity of the potential function $\Phi(Z)$ and its derivatives about $Z = 1$

As proceeded above, one expands $\Phi(Z)$ and its derivatives about $Z = 1$, making use of the auxiliary coordinate $Y = Z - 1$, with as many terms as necessary to achieve a given numerical accuracy:

$$\Phi(Z) \approx \left(-\frac{Y}{2} - \frac{Y^2}{8} + \frac{Y^3}{64} - \cdots \right) \mathrm{signal}(Z) \sqrt{\frac{2}{Y}} - \frac{1}{4} - \frac{1}{2\pi} - \left(\frac{1}{4} + \frac{1}{\pi} \right) Y + \frac{Y^2}{6\pi} - \cdots$$

(A.14)

$$\Phi'(Z) \approx \left(-\frac{1}{4} - \frac{3Y}{16} + \frac{5Y^2}{128} - \cdots\right) \text{signal}(Z)\sqrt{\frac{2}{Y}} - \frac{1}{4} - \frac{1}{\pi} + \frac{Y}{3\pi} - \frac{2Y^2}{5\pi} + \cdots \tag{A.15}$$

$$\Phi''(Z) \approx \left(\frac{1}{8Y} - \frac{3}{32} + \frac{15Y}{256} - \frac{35Y^2}{1024} + \cdots\right) \text{signal}(Z)\sqrt{\frac{2}{Y}} + \frac{1}{3\pi} - \frac{4Y}{5\pi} + \frac{46Y^2}{35\pi} - \cdots \tag{A.16}$$

Assuming, for simplicity, that the *sqrt* singularity occurs for the natural coordinate ξ at $\xi = 0$ (it is always possible to change coordinates when the singularity occurs at $\xi = 1$), the above equations may be expressed as the expansion about $Z = 1$:

$$\Phi(Z) \approx \Phi_{sqrt}(Z) / \sqrt{\xi} + \Phi_{reg}(Z) \tag{A.17}$$

$$\Phi'(Z) \approx \Phi'_{sqrt}(Z) / \sqrt{\xi} + \Phi'_{reg}(Z) \tag{A.18}$$

$$\Phi''(Z) \approx \Phi''_{sqrt}(Z) / \sqrt{\xi} + \Phi''_{reg}(Z) \tag{A.19}$$

where $\Phi_{sqrt}(Z)$, $\Phi'_{sqrt}(Z)$ and $\Phi''_{sqrt}(Z)$ can be inferred from Eqs. (A.14), (A.15) and (A.16). The potential function $\Phi(Z)$ presents a weaker singularity, $\sqrt{\xi}$, than its derivatives. However, the development of Eq. (A.14) shall present the structure of the derivatives of $\Phi(Z)$, as shown above, in such a way that the same numerical integration code, for singularity $\sqrt{1/\xi}$, can be used in all cases. The second derivative Φ'' of the potential function is required only for elasticity problems and is always multiplied, as for the semicrack 1, by $y_1 = r\sin(\theta - \theta_1)$, which is equal to zero at the crack tip, when $\theta = \theta_1$.

The signal function signal(Z) defined in Eq. (A.4) this time affects the non-regular parts of $\Phi(Z)$ and its derivatives. Then, it is advisable to evaluate $\Phi_{reg}(Z)$, $\Phi'_{reg}(Z)$ and $\Phi''_{reg}(Z)$ as in the expansions shown in Eqs. (A.14), (A.15) and (A.16) and obtain $\Phi_{sqrt}(Z)$, $\Phi'_{sqrt}(Z)$ and $\Phi''_{sqrt}(Z)$ by subtractions from the complete, non-expanded functions, such as

$$\Phi_{sqrt}(Z) = (\Phi(Z) - \Phi_{reg}(Z))\sqrt{\xi} \tag{A.20}$$

in the case of $\Phi(Z)$. This subtraction is simple and effective for a numerical implementation, as a quadrature algorithm will never make use of the abscissa $\xi = 0$.

A.4 Quadrature of a function with $1/\sqrt{\xi}$ singularity with the use of subintervals

This routine is similar to the one of Section A.2 and repeats several logical sequences with the purpose of clarity and self-containment. It carries out the numerical quadrature

$$F = \int_0^1 f(\xi)\,\mathrm{d}\xi \equiv \int_0^1 \left(f_{sqrt}(\xi)/\sqrt{\xi} + f_{reg}(\xi) \right) \mathrm{d}\xi \tag{A.21}$$

where both $f_{sqrt}(\xi)$ and $f_{reg}(\xi)$ have no embedded singularities but cannot be approximated by a low-order polynomial about $\xi = 0$. However, it is assumed that the function $f(\xi)$ can be approximated by a low-order polynomial about $\xi = 1$. As proposed, one is in principle dealing with an improper integral. However, this routine should be applied also in the case of $\lim_{\xi \to 0} f_{sqrt}(\xi) = 0$.

The interval $[0,1]$ is split into n_Δ subintervals of increasing magnitude counting from $\xi = 0$, such that $\Delta\xi_i = \alpha \Delta\xi_{i-1}$, for $i = 2..n_\Delta$. A special quadrature of $f_{sqrt}(\xi)/\sqrt{\xi}$ is carried out in the interval $[0, \Delta\xi_1]$ and a Gauss-Legendre quadrature evaluates the remaining parts of the integral in Eq. (A.9) along the successive, increasingly larger subintervals.

Input data. The input data for the algorithm are:

- Functions $f(\xi), f_{sqrt}(\xi)$ and $f_{reg}(\xi)$.
- Number of subintervals n_Δ (recommended value is $n_\Delta = 4$).
- Subinterval amplification factor α (recommended value is $\alpha = 2$).
- Data for the logarithm quadrature: number of abscissas n_q, abscissas $\xi_q[\,]$ and weights $w_q[\,]$ (recommended value is $n_q = 5$).
- Data for the Gauss-Legendre quadrature: number of abscissas n_g, abscissas $\xi_g[\,]$ and weights $w_g[\,]$ (recommended value is $n_g = 5$).

Ouput. The output of the algorithm is the numerical value F of the integral in Eq. (A.21).

Algorithm. Define the length and start point of the first interval:

$$\Delta\xi = \frac{\alpha - 1}{\alpha_\Delta^n - 1}; \quad \xi_i = 0 \tag{A.22}$$

- Evaluate $\int_0^{\Delta\xi} f(\xi)\,\mathrm{d}\xi$ numerically along the first interval by adequately splitting the integrand into regular and improper parts (and also taking care of interval normalization):

$$F = \Delta\xi \sum_{i=1}^{n_g} f_{reg}\left(\xi_g[i]\Delta\xi\right) w_g[i] + \sqrt{\Delta\xi} \sum_{i=1}^{n_q} f_{sqrt}\left(\xi_q[i]\Delta\xi\right) w_q[i] \tag{A.23}$$

  In this equation, $f_{sqrt}(\xi) = \left(f(\xi) - f_{reg}(\xi)\right)\sqrt{\xi}$.

- For a loop with $n_\Delta - 1$ repetitions, successively update the values of Eq. (A.22) as

$$\xi_i = \xi_i + \Delta\xi; \quad \Delta\xi = \alpha\,\Delta\xi \tag{A.24}$$

  and carry out the numerical evaluation of $\int_{\xi_i}^{\xi_i+\Delta\xi} f(\xi)\,\mathrm{d}\xi$:

$$F = F + \Delta\xi \sum_{i=1}^{ng} f\left(\xi_i + \xi_g[i]\Delta\xi\right) w_g[i] \tag{A.25}$$